International Geology Review

ISSN: 0020-6814 (Print) 1938-2839 (Online) Journal homepage: http://www.tandfonline.com/loi/tigr20

Metavolcanic host rocks, mineralization, and gossans of the Shaib al Tair and Rabathan volcanogenic massive sulphide deposits of the Wadi Bidah Mineral District, Saudi Arabia

John C. Volesky, Matthew I. Leybourne, Robert J. Stern, Jan M. Peter, Daniel Layton-Matthews, Sarah Rice & Peter R. Johnson

To cite this article: John C. Volesky, Matthew I. Leybourne, Robert J. Stern, Jan M. Peter, Daniel Layton-Matthews, Sarah Rice & Peter R. Johnson (2017) Metavolcanic host rocks, mineralization, and gossans of the Shaib al Tair and Rabathan volcanogenic massive sulphide deposits of the Wadi Bidah Mineral District, Saudi Arabia, International Geology Review, 59:16, 1975-2002, DOI: 10.1080/00206814.2017.1307789

To link to this article: http://dx.doi.org/10.1080/00206814.2017.1307789

INTERNATIONAL GEOLOGY REVIEW, 2017
VOL. 59, NO. 16, 1975–2002
https://doi.org/10.1080/00206814.2017.1307789

Taylor & Francis
Taylor & Francis Group

Metavolcanic host rocks, mineralization, and gossans of the Shaib al Tair and Rabathan volcanogenic massive sulphide deposits of the Wadi Bidah Mineral District, Saudi Arabia

John C. Volesky[a], Matthew I. Leybourne[b], Robert J. Stern[a], Jan M. Peter[c], Daniel Layton-Matthews[d], Sarah Rice[e] and Peter R. Johnson[f]

[a]Geosciences Department, University of Texas at Dallas, Richardson, TX, USA; [b]Mineral Exploration Research Centre, Harquail School of Earth Sciences, Laurentian University, Sudbury, Canada; [c]Central Canada Division, Geological Survey of Canada, Ottawa, Canada; [d]Geological Sciences and Geological Engineering, Queens University, Kingston, Ontario, Canada; [e]ALS Geochemistry, North Vancouver, Canada; [f]UT Dallas, Portland, OR, USA

ABSTRACT

The Wadi Bidah Mineral District of Saudi Arabia contains more than 16 small outcropping strata-bound volcanogenic Cu–Zn–(Pb) ± Au-bearing massive sulphide deposits and associated zones of hydrothermal alteration. Here, we use major and trace element analyses of massive sulphides, gossans, and hydrothermally altered and least altered metamorphosed host rock (schist) from two of the deposits (Shaib al Tair and Rabathan) to interpret the geochemical and petrological evolution of the host rocks and gossanization of the mineralization. Tectonic interpretations utilize high-field-strength elements, including the rare earth elements (REE), because they are relatively immobile during hydrothermal alteration, low-grade metamorphism, and supergene weathering and therefore are useful in constraining the source, composition, and physicochemical parameters of the primary igneous rocks, the mineralizing hydrothermal fluid and subsequent supergene weathering processes. Positive Eu anomalies in some of the massive sulphide samples are consistent with a high temperature (>250°C) hydrothermal origin, consistent with the Cu contents (up to 2 wt.%) of the massive sulphides. The REE profiles of the gossans are topologically similar to nearby hydrothermally altered felsic schists (light REE (LREE)-enriched to concave-up REE profiles, with or without positive Eu anomalies) suggesting that the REE experienced little fractionation during metamorphism or supergene weathering. Hydrothermally altered rocks (now schists) close to the massive sulphide deposits have high base metals and Ba contents and have concave-up REE patterns, in contrast to the least altered host rocks, consistent with greater mobility of the middle REE compared to the light and heavy REE during hydrothermal alteration. The gossans are interpreted to represent relict massive sulphides that have undergone supergene weathering; 'chert' beds within these massive sulphide deposits may be leached wall-rock gossans that experienced silicification and Pb–Ba–Fe enrichment from acidic groundwaters generated during gossan formation.

ARTICLE HISTORY
Received 6 April 2016
Accepted 8 March 2017

KEYWORDS
Massive sulphide; gossan; subduction; hydrothermal alteration; mineral exploration; Saudi Arabia; rare earth element; Wadi Bidah Mineral District

Introduction

Volcanogenic massive sulphide (VMS) deposits are major sources of Cu, Zn, Pb, and Ag (±Au) globally, and have formed throughout Earth history (e.g. Hannington *et al*. 2005; Lydon 2007). Volcanogenic massive sulphide deposits form in a variety of tectonic settings, including backarc and intra arc basins and mid-ocean ridges (Tornos *et al*. 2015). High temperature black smoker venting was initially discovered on mid-ocean ridges in the 1970s and much subsequent research, therefore, looked at the mid-ocean ridges as modern analogues for ancient, now on-land, VMS. However, more recent work on modern arcs and back-arcs (Craddock and Bach 2010; de Ronde *et al*. 2011) indicates that rifted arc and back arc settings are better analogues for VMS in the ancient rock record (Hannington *et al*. 2005). Understanding the tectonic environment of formation of VMS deposits is important for understanding the evolution of Earth through time, and for developing better exploration models.

The Wadi Bidah Mineral District (WBMD) in the Asir terrane of the Arabian Shield, southern Saudi Arabia,

CONTACT Matthew I. Leybourne mleybourne@laurentian.ca Mineral Exploration Research Centre, Harquail School of Earth Sciences, Laurentian University, Sudbury, Ontario P3E 2C6, Canada

Supplemental data for this article can be accessed here.

contains over 16 polymetallic VMS occurrences including small, well-exposed, stratabound, volcanogenic copper and gold-bearing massive sulphide deposits, and associated zones of hydrothermal alteration (Volesky *et al*. 2003). Much attention has been focused on the Arabian–Nubian Shield (ANS) in terms of understanding its tectonic setting and accretion history (e.g. Abdelsalam *et al*. 2002; Hargrove *et al*. 2006; Stoeser and Frost 2006; Fritz *et al*. 2013; Stern *et al*. 2013). However, relatively little is known about the style of mineralization and associated host-rock alteration (Sangster and Abdulhay 2005), formation of associated gossans and the tectonic setting of the host metavolcanic rocks of the Asir Terrane (Bamousa 2013; Hamimi *et al*. 2014), and the WBMD (Volesky *et al*. 2003).

Herein, we focus on two representative deposits (Shaib al Tair (SAT) and Rabathan) using major and trace element geochemical data to characterize the chemical composition of the massive sulphides, gossans derived from these massive sulphides, associated zones of hydrothermal alteration and metamorphosed host rocks, and interpret the geochemical and petrological evolution of the massive sulphide deposits and host rocks. We focus on the high-field-strength elements (HFSE) and the rare earth elements (REE) because they are relatively immobile during low-grade metamorphism and weathering, and are therefore useful as indicators of sedimentary and igneous protolith composition (Hanson 1980; McLennan 1989), and in providing constraints on volcanic rock tectonic setting as well as the nature, source, and composition of ore-forming hydrothermal fluids (e.g. Klinkhammer *et al*. 1994; Leybourne *et al*. 2006; Reeves *et al*. 2011).

The specific objectives of the present study are to: (1) determine the palaeotectonic setting in which the mafic and felsic schist protoliths and mineralization occurred; (2) elucidate the genetic processes that formed Wadi Bidah VMS; (3) determine the origin of the Fe-rich gossans; and (4) develop geochemical vectors useful for finding concealed mineralization.

Tectonic setting and geology of the WBMD

The WBMD is located in the western part of the Neoproterozoic (900–550 Ma) Asir Terrane, one of the tectonostratigraphic units that make up the Arabian Shield (Figure 1; Camp 1984, Stoeser and Camp 1985). The terranes comprise Tonian and Cryogenian intra-oceanic arc/back-arc basin complexes and microcontinents juxtaposed along N- and E-trending sutures that are overprinted by Ediacaran collision-related structures (Figure 1; Abdelsalam and Stern 1996). Volcanogenic massive sulphide base metal mineralization occurs in all the terranes of the Arabian Shield (Agar 1992) and equivalent rocks in the Nubian Shield, west of the Red Sea (Figure 1). These VMS deposits represent base-metal ± gold–silver mineralization of the type commonly occurring in submarine arcs and backarc basins and which is associated with convergent plate margins. Many examples are classic VMS deposits; others are highly sheared and are of unknown or uncertain deposit type. The ANS juvenile arc–backarc basin rocks also host: (1) epithermal gold deposits; (2) Fe(oxide)–Au deposits; (3) Ni–Co and Cr associated with mafic-ultramafic rocks in local extensional or back-arc settings; and (4) banded iron formation. Overall, ANS sulphide deposits are hosted by Tonian and Cryogenian lithologic assemblages that range from about 850 Ma in the WBMD (the topic of this article), the Shwas mineral district east of WBMD, and the Bisha (Barrie *et al*. 2007) and Asmara mineral districts in the south-central Nubian Shield, to about 700 Ma in the eastern part of the Arabian Shield (Doebrich *et al*. 2007). Apart from the WBMD occurrences described here, classic VMS occurrences in the Arabian Shield include Al Masane and Jabal Sayid (Sangster and Abdulhay 2005). Umm ad Damar, Ash Shizm, Farah Garan, and Jabal Baydan are smaller, but poorly explored VMS deposits. Weathering zones of some VMS deposits, enriched in supergene gold, have previously been worked as gold mines at Al Hajar and are presently being worked at Jadmah (Cottard *et al*. 1994), and these are economically favourable features of VMS deposits in the Nubian Shield (Cottard *et al*. 1986).

The WBMD is a N-trending belt, 70 km long and 20 km wide, located between latitudes 20° and 21° N and longitudes 41° 10′ and 41° 30′ E (Figure 2). The WBMD is subdivided from east (oldest) to west (youngest) into three major lithological groups. Group 1: mafic volcanic rocks; group 2: felsic volcaniclastic rocks; and group 3: felsic volcaniclastic and epiclastic rocks (Beziat and Donzeau 1989). Group 1 is assigned to the Khumrah Greenstone, and groups 2 and 3 are assigned to the Hawiyah Formation (Ziab and Ramsay 1986; Johnson 1999). Regional metamorphism in the WBMD attained greenschist facies (Beziat and Donzeau 1989). Intrusive rocks of the WBMD range in composition from gabbro to granite.

Previous geochemical studies of the WBMD have focused on evaluating the economic potential of base and precious metal deposits, classifying igneous rocks using major and trace element data, and using geochemistry to infer the palaeotectonic setting. Jackaman

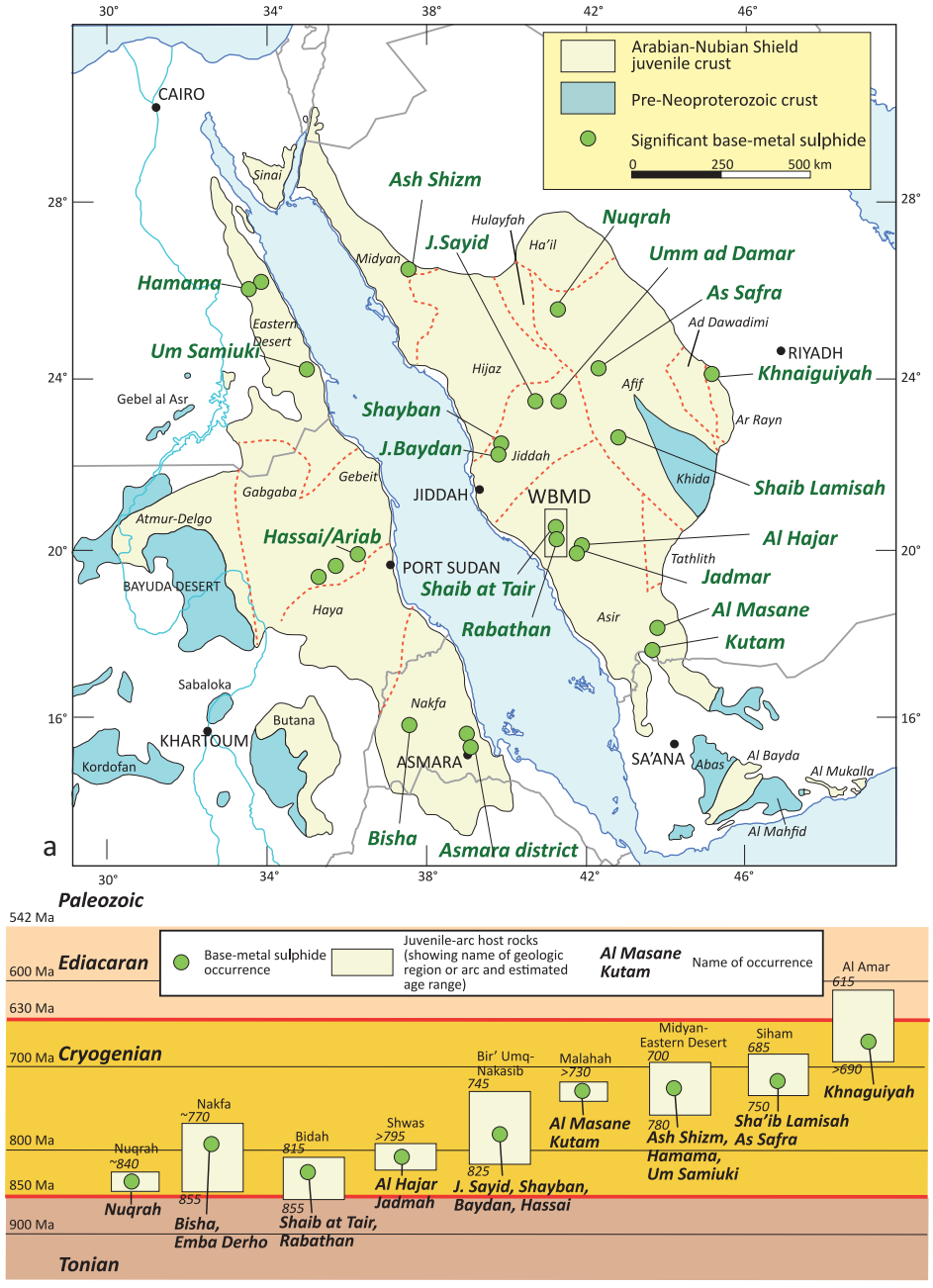

Figure 1. Location of Wadi Bidah Mineral District within the Asir terrane of the Arabian Shield (Stoeser and Camp 1985) and major sulphide occurrences in the Arabian-Nubian Shield including typical VMS as well as Cu–Zn sulphide occurrences of uncertain deposit type. (a) Distribution of sulphide occurrences showing their location in most terranes in the shield. (b) Time-spread of occurrences in the ANS showing a preferential concentration in the Cryogenian, based on the assumption that the sulphide occurrences are broadly coeval with their host rocks.

(1972) and Greenwood *et al*. (1976; 1980) recognized the tholeiitic affinity of Wadi Bidah basalt (group 1). Ramsay *et al*. (1981) and Lemiere (1989) confirmed the tholeiitic character of the WBMD basalts and concluded that the palaeotectonic setting was an island arc.

The massive sulphide deposits of the WBMD have surface expressions of iron-rich caps or gossans and associated zones of hydrothermal alteration. Volesky *et al*. (2003) identified gossans and zones of hydrothermal alteration using spectral analysis of Landsat EM and ASTER remote sensing data. The gossans, hydrothermally altered host rocks, and metamorphosed host rocks all have distinct spectral signatures that allow the lithologies to be differentiated based on band ratios.

Volesky *et al*. (2003) showed that the WBMD, including the massive sulphide deposits and host rocks, has been folded and sheared by post-mineralization

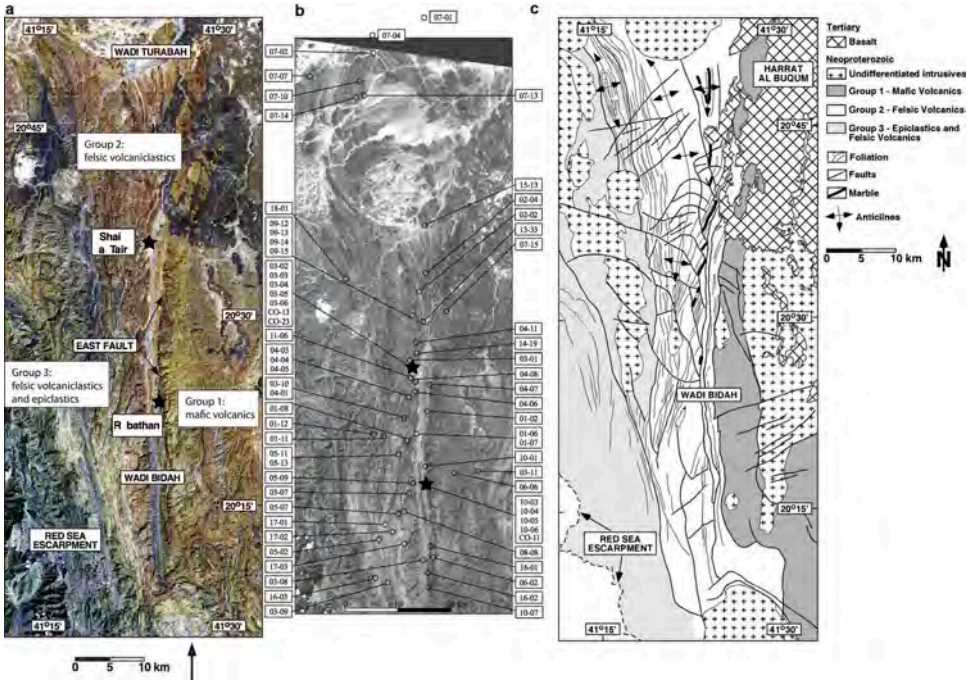

Figure 2. (a) Landsat ETM+ (7–5–4) colour composite image using the convention (R–G–B) of the WBMD indicating the locations of the Shaib al Tair (SAT) and Rabathan prospects. (b) Landsat 7 (Banc 8) grey-scale image of the WBMD indicating locations of rock samples used in this study. (c) Geology map with major structures, from Volesky *et al*. (2003).

deformation, which variably obscures the primary relationships between the mineralization and the host rocks. All the known WBMD VMS deposits are hosted by group 2 felsic volcaniclastic rocks (Figure 3; Volesky *et al*. 2003). The age of these rocks and their VMS deposits is between 855–815 Ma, the age of Dhuqiyah complex, which intrudes the Wadi Bidah rocks (Fleck and Hadley 1982; Radain *et al*. 1987). Jackaman (1972) characterized the massive sulphide deposits of the WBMD as stratabound lenses of pyrite, chalcopyrite, and sphalerite. These massive sulphide deposits have been known for at least 1200 years, based on the presence of archaeological ruins and slag dumps located near several of them (Jackaman 1972).

The WBMD massive sulphide deposits are interpreted to be stratiform (Jackaman 1972; Beziat and Donzeau 1989). Due to the deformation, the extent to which the massive sulphides were precipitated at the seafloor in a mound or in the subseafloor as replacements (Genna *et al*. 2014b; Piercey 2015; Tornos *et al*. 2015) is unclear. Furthermore, the massive sulphides are thought to have been deposited near a backarc basin spreading centre, based on stratigraphic relationships established by Volesky *et al*. (2003) and the tectonic interpretation of Camp (1984), who suggested that the Khumrah Greenstone was the product of rifting to open what he called the Bidah inter-arc basin. The WBMD sulphide deposits occur in two belts (Beziat and Donzeau 1989). Proximal deposits (close to the site of hydrothermal discharge at the palaeoseafloor) occur in a belt west of Wadi Bidah, and include the Gehab, SAT, and Mulhal deposits (Sangster and Abdulhay 2005). These occur at the same stratigraphic position – approximately two km to the west – relative to a distinctive marble unit. Distal deposits (further from the site of hydrothermal discharge at the palaeoseafloor) occur in a belt east of Wadi Bidah and include the Abu Sulal and Rabathan deposits. Distal and proximal deposits both appear to be confined to a single stratigraphic horizon, so the deposits may have been associated with the same felsic volcanic episode and have subsequently been folded and faulted into their present position (Volesky *et al*. 2003).

The two deposits studied here are representatives of both proximal (SAT) and distal (Rabathan) deposits. The dominant rock type in the Rabathan area is calcareous quartz schist, with carbonate and quartz disseminations and beds up to 1 m thick (Figure 4; Sangster and Abdulhay 2005). Mineralization at the Rabathan deposit is localized in a north-plunging fold hinge with massive and disseminated sulphides in carbonatized felsic schists and so-called 'cherty-ferruginous beds' (Figure 4; Sangster and Abdulhay 2005). Kiilsgaard *et al*. (1978) calculated reserves of the Rabathan R4 prospect at 1.5 Mt grading 2.3% Cu, 0.03% Zn, 285 g/t

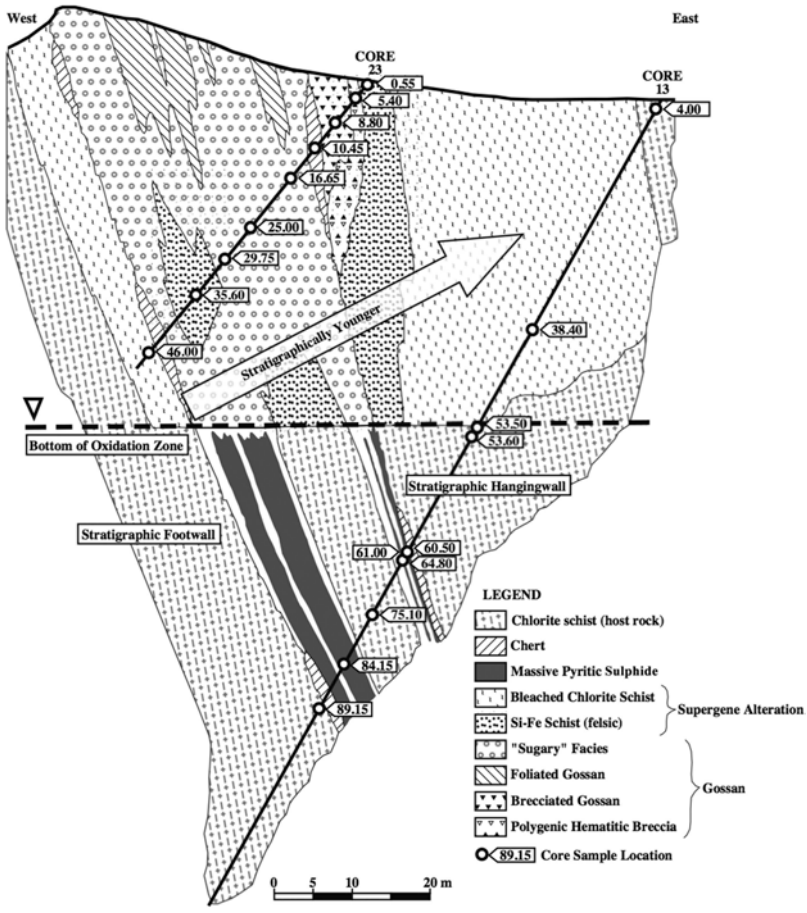

Figure 3. Simplified geologic cross-section of the SAT prospect indicating the traces of the drillholes and locations of core sample analysed in this study (modified from Coumoul *et al*. 1989).

Ag, and 0.16 g/t Au. Riofinex Geological Mission (1979) calculated combined reserves of the R4 and R3 prospects at 2.1 Mt grading 2.5% Cu, 0.5% Zn, 1.5 g/t Ag, and 1.2 g/t Au. Further work by Koch-Mathian *et al*. (1994) reported indicated and inferred reserves of 1.3 Mt grading 2.88% Cu. The main sulphide minerals are pyrite and chalcopyrite with minor sphalerite, pyrrhotite, and magnetite. Sulphides are present as banded layers intercalated with quartz–chlorite–dolomite schist, clastic sulphides, and microbrecciated sulphide (Koch-Mathian *et al*. 1994).

The main lithology that hosts mineralization at SAT is chlorite–quartz schist (Figure 4). Mineralization occurs as beds of massive and disseminated pyrite with minor chalcopyrite (Sangster and Abdulhay 2005). Barite is a common gangue mineral and sphalerite is more common within the eastern side of the deposit, which contains up to 4.8 % Zn. At SAT, Earhart and Mawad (1970) estimated the main sulphide body (400 m long by 29 m wide, extending 80 m down-dip below the oxidized zone) to contain 4 Mt grading 0.37% Cu and 0.5% Zn; Riofinex Geological Mission (1979) revised this estimate to 2.4 Mt at similar grades (Sangster and Abdulhay 2005).

Sampling and methods

Sampling

Fieldwork was conducted in February of 2000 and included locating known deposits in the WBMD, collecting rock and mineralization samples, collecting structural data, and recording GPS locations of field data and control points for georeferencing Landsat ETM+ and ASTER remote sensing scenes (Volesky, 2002). The GPS positions were later differentially corrected to increase accuracy of positions from ±100 to ±5 m. Control points were features in the field that could easily be identified on the Landsat ETM+ and ASTER images (e.g. road intersections, concrete dams with a reservoir). Rock samples (120 samples) were selected on the basis of the following criteria: (1) having distinct spectral characteristics or appearance based on analysis of remote sensing images; (2)

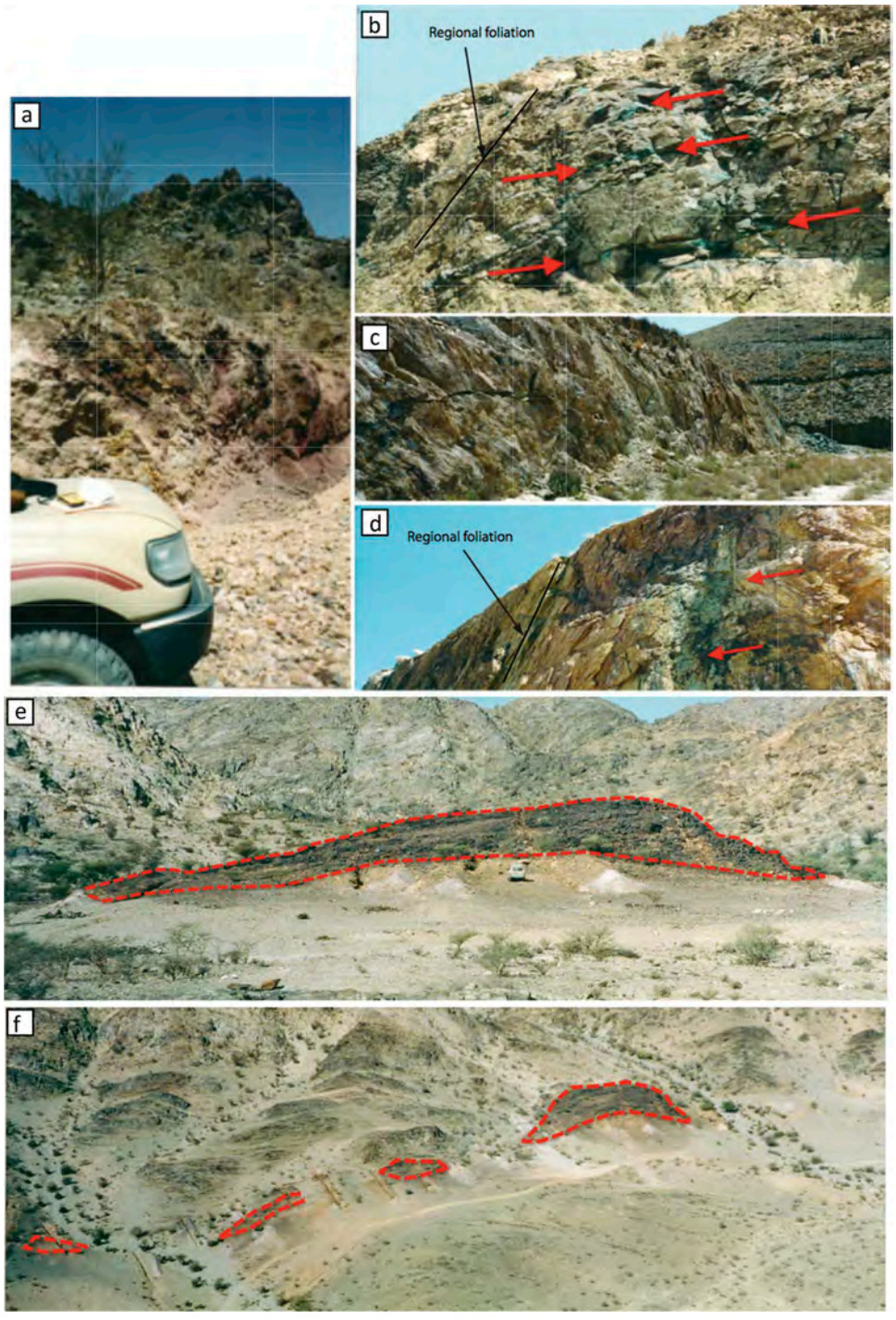

Figure 4. (a) Rabathan gossan (sample 10-05); (b) Rabathan chert with Cu mineralization (malachite) (sample 10-06a) along subhorizontal joints (red arrows) oblique to the steeply dipping regional foliation; (c) altered felsic schist (sample 17-02b); (d) altered felsic schist with Cu mineralization; note the steep dip of the schistosity; (e) SAT, north to the right; dotted line approximate outline of gossan. The felsic schist outcrop west of the gossan, in the footwall of the mineralized zone, shows a well-developed gently south-plunging lineation reflecting the southerly plunge of the regional folding; (f) SAT from helicopter, north to the right; showing exploration trenches and approximate outline of gossan.

outcrops of massive sulphide deposits/gossans and associated zones of hydrothermal alteration (e.g. Figure 4); (3) host rock collected from transects across the massive sulphide deposits; and (4) diamond drill core (prefixes CO-11, 13, and 23) from the SAT and Rabathan prospects (Figure 2) collected from the Saudi Geological Survey core library. The cross-section of the SAT deposit shows the locations and lithologies of the

respective core samples (Figure 3). Cores were drilled by the Bureau de Recherches Geologique et Minieres in October and December 1987.

Mineralogy and petrography

X-ray diffraction (XRD) analysis was used to determine the bulk mineralogy of 30 rock samples. XRD analyses were performed utilizing a Rigaku® or Scintag® automated powder diffractometer equipped with a Cu X-ray radiation source (40 kV, 35 mA) and a solid-state or scintillation detector. Semi-quantitative determinations of whole-rock mineral contents were done utilizing integrated peak areas (derived from peak-decomposition/profile fitting methods) and empirical reference intensity ratio factors determined specifically for the diffractometer used in data collection. Observations of 22 standard petrographic thin sections with a transmitted light microscope were used in conjunction with XRD analysis to determine the mineralogy of the rock samples.

Sample processing for geochemical analysis

Rock samples (~110 samples) were processed in the Geosciences Department at the University of Texas at Dallas (UTD). Samples were first coarsely crushed using a jaw crusher. Samples were then run through a rock chipper, and finally pulverized to <200 mesh in a SPEX® pulverizer using an alumina container and balls. Rocks were dissolved for chemical analysis in the geochemistry laboratory at UTD using a lithium-meta/tetraborate method. Rock powders were ignited at 900°C for four hours to determine loss on ignition, a process that converted all Fe to Fe^{3+}. Two tenths of a gram of rock powder were then combined with 0.6 g of lithium meta/tetraborate flux and fused at 900°C. Molten beads were quenched and dissolved in 4% HNO_3-EDTA solution. The solution was diluted to 100 ml and filtered. Filtrate was collected and used to prepare samples with a final dilution factor of 4000. Samples were processed in sets of 10 (8 samples, 1 certified reference material (CRM) standard, 1 method blank). The CRMs used were BHVO-2 (Hawaiian Basalt), GSP-2 (Silver Plume Granodiorite), G-2 (Granite), and RGM-1 (Glass Mountain Rhyolite).

A subset of samples (n = 33) were analysed at ALS Geochemistry, North Vancouver, B.C., Canada for trace and rare earth elements following lithium metaborate fusion and digestion in nitric acid (ALS method ME-MS81). For sulphide-rich samples, a four acid digestion was used (ME-MS61r). For 10 of the samples reanalysed, the pulps from UTD were used. For the remaining 23 samples, the analyses represent pulverization of different splits.

Analytical methods

At UTD, digested solutions were analysed for major and minor elements (Si, Ti, Al, Fe, Mn, Mg, Ca, Na, K, Ba, and Sr) on a Perkin-Elmer Optima 3300 dual view Inductively Coupled Plasma Optical Emission Spectrometer (ICP-OES). Solutions were analysed for trace elements (Cr, Ni, Cu, Zn, Rb, Y, Zr, Nb, La, Ce, Pr, Nd, Sm, Eu, Tb, Gd, Dy, Ho, Er, Tm, Yb, Lu, Pb, Th, and U) on a Perkin Elmer–Sciex Elan 6100 Dynamic Reaction Cell Inductively Coupled Plasma Mass Spectrometer (DRC-ICP-MS). Certified reference material (CRM) standards and method blanks (Supplementary Table 1) were run concurrently with the WBMD rock samples to check analytical results and to detect and correct determinate method errors.

At ALS Geochemistry (see Supplementary Table 2 for CRM data), rock solutions were analysed on an Elan 9000 ICP-MS; special care was taken to minimize oxide formation, using inter-element correction (IEC) standards and algorithms to adjust for BaO^+ interferences on ^{151}Eu and ^{153}Eu, given the barium-rich nature of some of the samples, as discussed below. It should be noted that samples with Ba/Eu > ~2000 have Eu contents that also reflect BaO^+ production in the plasma. Consequently, Eu contents for samples with Ba/Eu >2000 (UTD analyses) are not used in this study.

Results

Mineralogy and alteration

Based on field identification, thin sections, and results from X-ray diffraction analysis (Supplementary Table 3), samples have been separated into two groups: (1) mafic and felsic schist, and (2) samples associated with mineral deposits (gossans, massive sulphides, and highly siliceous rocks referred to here as chert). Schists are separated into two subgroups: mafic (plagioclase–quartz–epidote–chlorite schists) and felsic (muscovite–chlorite–quartz schists). Samples associated with mineral deposits are separated into subgroups: (1) massive sulphides (containing pyrite, sphalerite, and quartz) east and west of Wadi Bidah (note that we consider samples with >25 vol.% sulphide to be 'massive sulphide'); (2) gossans (dominantly goethite, haematite, quartz, and lesser natrojarosite, jarosite, and barite) grading laterally into ferruginous chert (dominantly quartz and haematite) east and west of Wadi Bidah; and (3) pyrolusite (± quartz and garnet), siderite and malachite-rich samples (Supplementary Table 3).

The mafic schists have been pervasively altered to an assemblage dominated by quartz–epidote–chlorite ± carbonate with variable plagioclase contents. Primary

igneous textures have typically been destroyed by deformation. A quartz–muscovite assemblage with minor chlorite and epidote dominates samples of felsic schists, which typically have a strong foliation defined by muscovite. Chert samples are dominated by quartz with variable iron oxide alteration and muscovite. The term 'chert' is a field description representing distal silica-rich portions of the gossans around the WBMD (Riofinex 1979).

Geochemical data

Using the sample preparation and analytical procedures outlined above, major element analysis of the CRMs generated results that are within the published ranges for each of the parameters measured. Major element totals for the CRMs are 100 ± 1% and the LOI for each CRM is approximately 1%. Standard deviations for the parameters measured are comparable to certified values. The WBMD samples are weathered, metamorphosed, and hydrothermally altered, and these processes have induced changes in mineralogy of the rocks and can produce indeterminate errors and increase LOI values. Major element totals for WBMD rocks are more variable than the CRMs with 66% of the WBMD samples having totals of 100 ± 2.5% and 90% of the samples having totals of 100 ± 5%. Because many of the samples are hydrothermally altered, and this is key to this study, the samples have been plotted without renormalization to 100% volatile-free. Major element totals may be low if the sample has high Ba, Cu, Pb, or Zn contents, because these elements are not included in the calculation of the total. Sulphur is volatile and is, therefore, included in the LOI values. Using the sample preparation and analytical procedures outlined above, trace element analyses of CRMs generated results, which are generally within the accepted ranges for the parameters measured.

Given the highly altered nature of most of the host rock samples analysed, we have classified the rocks using the Zr/TiO_2 *versus* Nb/Y diagram of Winchester and Floyd (Figure 5; 1977). The WBMD volcanic rocks and their metamorphosed equivalents mostly plot as subalkaline mafic to felsic rocks. Samples identified as mafic schists in the field chiefly plot as subalkalic basalts, whereas felsic schists mainly plot as subalkalic andesites despite generally high (up to 90 wt.%) SiO_2 contents. Some of the samples classified as felsic schists in the field with high (84–92.5 wt.%) SiO_2 contents have low Zr/TiO_2, owing to low Zr contents, and these are probably metasediments (volcaniclastic), dominated by quartz.

The Fe/Ti *versus* Al/(Al + Fe + Mn) diagram can be used to differentiate hydrothermal from hydrogenous and detrital deposits (Figure 6(a); Boström 1973, Peter and Goodfellow 1996). Chemical sediments or hydrothermal precipitates formed from high-temperature (300–400°C) hydrothermal fluids have low Al contents and high Fe/Ti values (Boström and Peterson 1969). The Fe/Ti values for the WBMD massive pyrite and gossan samples are >30 and for the schists (host rocks) are <50. The Al/(Al + Fe + Mn) value is an index of the relative proportion of detrital clay (ratioed to clay plus Fe and Mn that are predominantly of hydrothermal origin); Al/(Al + Fe + Mn) >0.4 is considered to indicate a detrital source in marine sediments (Boström and Peterson 1969; Boström 1973; Peter *et al*. 2003). Most of the mafic and felsic schists plot in the detrital and modern volcanic arc field, with Al/(Al + Fe + Mn) values >0.4, whereas the massive pyrite, gossan, and chert samples plot in the hydrothermal field with Al/(Al + Fe + Mn) values <0.1 (Figure 6(a)). The less altered schists plot near the field of modern volcanic rocks, whereas with increased alteration, they shift to lower Al/(Al + Fe + Mn) and higher Fe/Ti. The extent of alteration of the felsic schists in particular is evident from the relative decrease in CaO + Na_2O compared to K_2O and Al_2O_3, whereas the mafic schists are similar in composition to average island arc type mafic rocks, suggesting that the mafic schists are less altered than the felsic schists (Figure 6(b)).

Felsic schists

The felsic schists from both deposits are characterized by elevated SiO_2 contents, ranging from 66.09 to 92.51 wt.% (Figure 7(a)). Most of the felsic schists have Al_2O_3 contents between 8.7 and 17.6 wt.%, although a few have Al_2O_3 as low as ~1 wt.% (Figures 7(c) and 8(b)). The effects of alteration and gossan development are evident in the range in $Fe_2O_3^T$ contents, up to 12.80 wt.%. Barium is highly variable, ranging from 20 to 28,926 ppm (average = 2399 ppm), whereas Sr and Rb are less variable, with much lower contents; Sr up to 891 ppm (average = 141 ppm) and Rb up to 73 ppm (average = 14 ppm). The HFSE have generally low abundances in these high silica rocks, with Zr ranging from 1.20 to 508 ppm (average = 57 ppm), Y ranging from 0.7 to 117 ppm (average = 15 ppm), Nb ranging from 0.05 to 27.7 ppm (average 3.4 ppm) and Th ranging from 0.05 to 7.45 ppm (average = 1.11 ppm). The VMS-associated metal contents are highly variable in the felsic schists, consistent with addition of Fe_2O_3 and Ba (i.e. dilution). Copper ranges from 11.5 to 2850

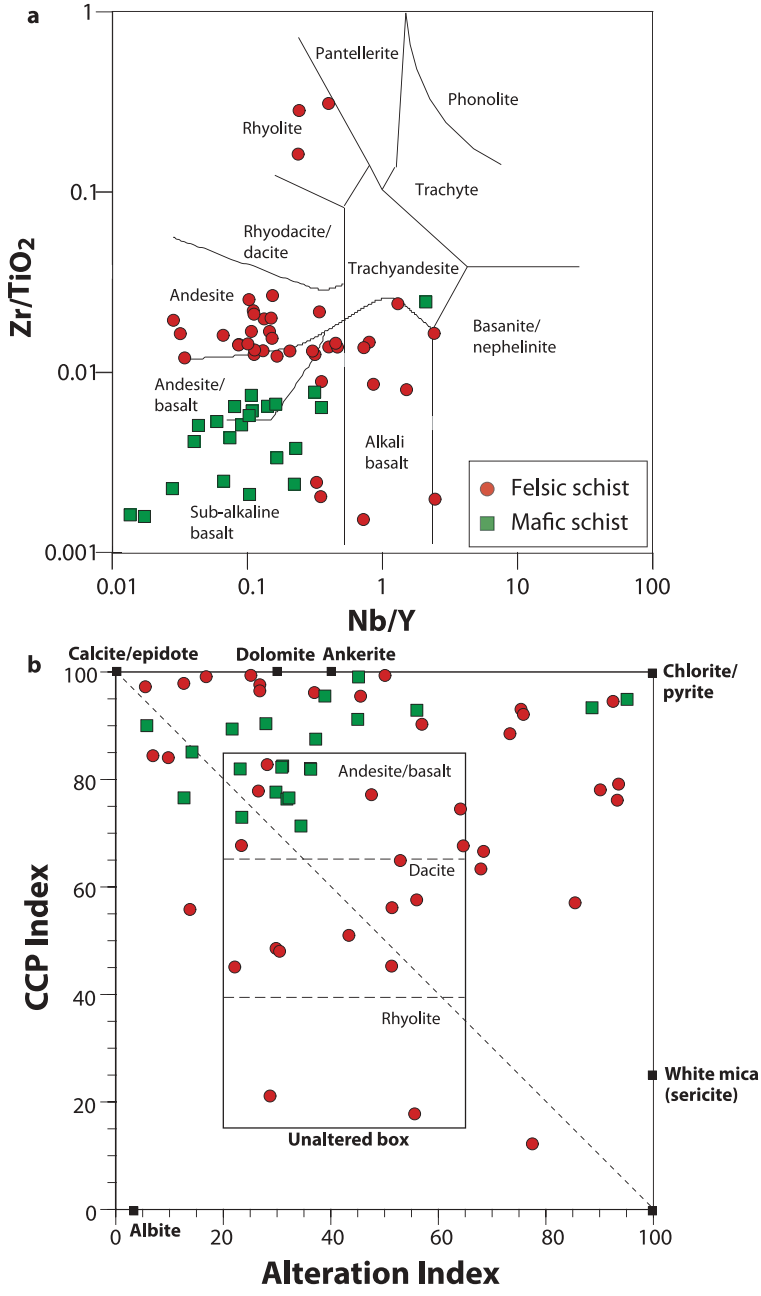

Figure 5. (a) Zr/TiO_2 *versus* Nb/Y classification diagram of Winchester and Floyd (1977). (b) Chlorite–carbonate–pyrite index (CCPI) *versus* alteration index (AI) plot (after Large *et al*. 2001a) showing the extent of alteration for many of the samples in this study, with a trend to the chlorite/pyrite alteration corner. Footwall sills and many flows and dikes plot as unaltered, however. CCPI = 100(MgO + FeO)/(MgO + FeO + Na_2O + K_2O); AI = 100(K_2O + MgO)/(K_2O + MgO + Na_2O + CaO). Data from Supplementary Table 4.

ppm (average = 275 ppm), Zn from 6.6 to 1637 ppm (average = 154 ppm) and Pb from <1 to 1445 ppm (average 83 ppm).

The felsic schists have predominantly flat to slightly LREE-enriched chondrite-normalized REE patterns, with $[La/Yb]_{cn}$ ranging from 0.14 to 21.4 and averaging 6.75 (Figure 9).

Cerium anomalies were calculated for the felsic schists using the formula:

$$Ce/Ce^* = \frac{[Ce_{sample}/Ce_{chondrite}]}{\sqrt{[La_{sample}/La_{chondrite}] \times [Pr_{sample}/Pr_{chondrite}]}}.$$

Most felsic schists have small negative Ce anomalies (average Ce/Ce* = 0.85), with an overall range of 0.43–1.48 (Figure 9(a)). Europium anomalies were also calculated for the felsic schists as

$$Eu/Eu^* = \frac{[Eu_{sample}/Eu_{chondrite}]}{\sqrt{[Sm_{sample}/Sm_{chondrite}] \times [Gd_{sample}/Gd_{chondrite}]}}.$$

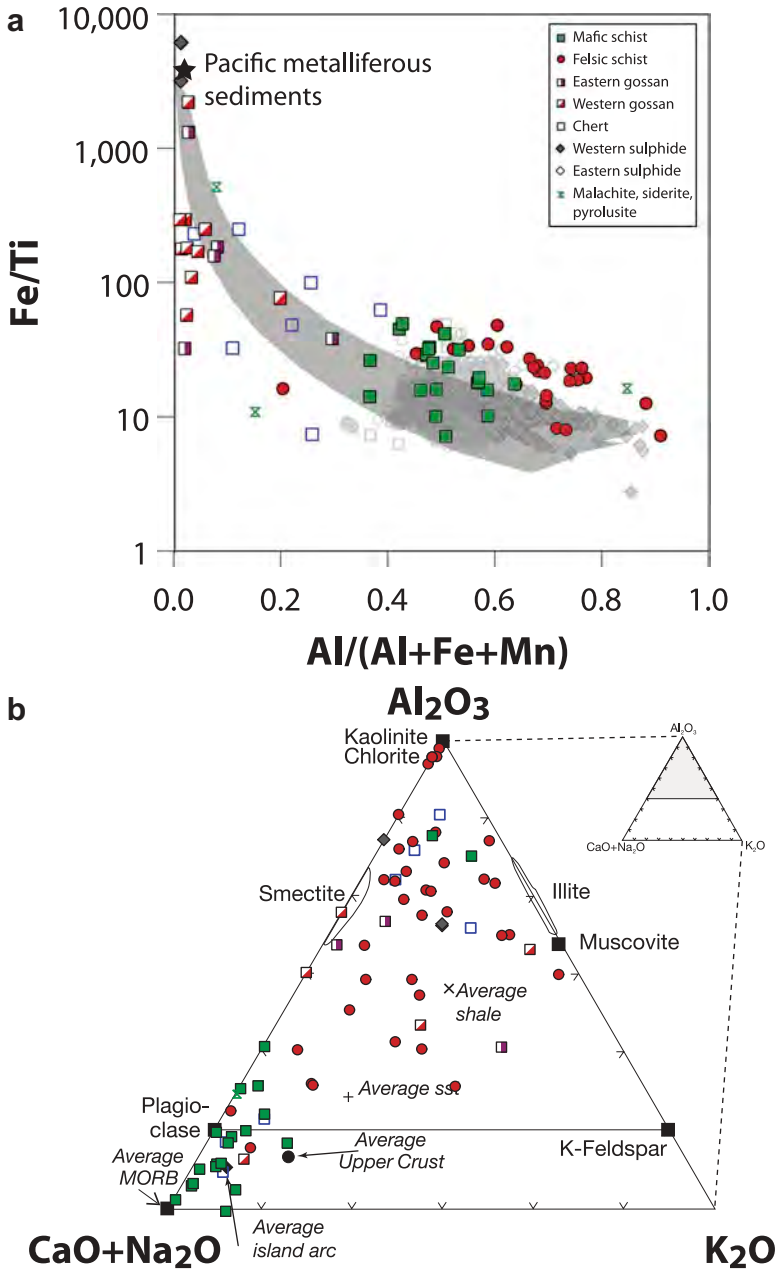

Figure 6. (a) Fe/Ti *versus* Al/(Al + Fe + Mn) bivariate plot for WBMD samples (after Boström 1973). This plot is used to estimate the hydrothermal and detrital sedimentary contributions to sediments. Also shown are ideal mixing curves between endmember hydrothermal sediment (Red Sea metalliferous sediments) and least altered mafic to felsic volcanic rocks from the modern Kermadec arc for reference (Wysoczanski, unpublished compilation). (b) Ternary plot of molecular proportions of Al_2O_3–CaO + Na_2O–K_2O (A–CN–K) showing positions of major minerals and sedimentary and volcanic rocks (modified after Nesbitt and Young 1982). Data from Supplementary Table 4.

Europium anomalies for the felsic schists range from negative to positive, 0.44–1.77 (average = 0.99).

Hydrothermally altered schists close to the most westerly massive sulphide horizons (Figure 3) possess similar REE abundances to the mafic schists and least altered schists but are characterized by concave-up REE patterns with $[La/Sm]_{cn}$ >1 and $[Gd/Yb]_{cn}$ <1 (Figures 9(a) and 10(b)). The felsic schists are characterized by high Ba/Eu, $[La/Sm]_{cn}$, $[Ba/Nb]_{pm}$, and Nb/Yb and lower $[Gd/Yb]_{cn}$ compared to the other rocks (Figure 10(a–f)). On a primitive mantle-normalized trace element plot, the felsic schists display negative Nb anomalies, with significant enrichments in Ba, U, and Pb compared to adjacent elements (Figure 11(a)).

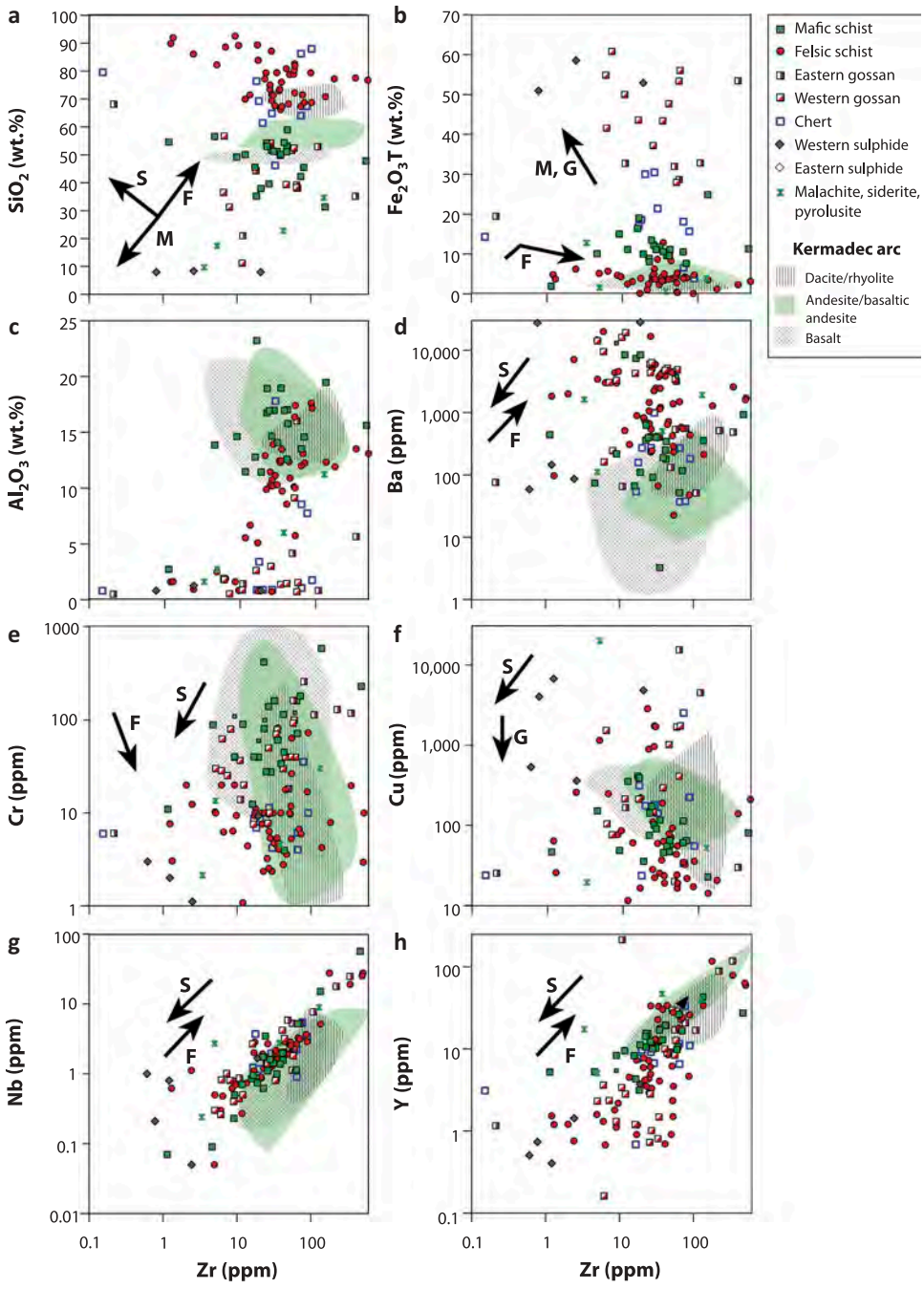

Figure 7. Bivariate plots of major and trace elements *versus* Zr content; Zr is relatively immobile during hydrothermal alteration and weathering and is therefore a good measure of igneous fractionation. (a) SiO_2 *versus* Zr; (b) $Fe_2O_3^T$ *versus* Zr; (c) Al_2O_3 *versus* Zr; (d) Ba *versus* Zr; (e) Cr *versus* Zr; (f) Cu *versus* Zr; (g) Nb *versus* Zr; (h) Y *versus* Zr. Data from Supplementary Table 4. Also shown are fields for basalts, basaltic-andesite/andesite and dacite/rhyolite from the Kermadec arc (data from Wysoczanski, unpublished). General trends for crystal fractionation (F), silicification (S), gossanization (G), and massive sulphide mineralization (M) are also shown.

Mafic schists

Mafic schists from both deposits are generally less altered than the felsic schists, based on their REE profiles and mobile major element contents, although the primary igneous minerals have been replaced by a quartz–chlorite–epidote assemblage (Supplementary Table 3). The SiO_2 contents range from 31.2 to 58.9 wt.% (average = 48.3) (Figures 7(a) and 8(a)). Mafic schists with low SiO_2 contents have either high $Fe_2O_3^T$ (oxides and/or sulphides in thin section; Figure 8(a)) or high CaO and LOI, consistent with the presence of calcite observed in thin section. Iron oxide contents are variable, ranging up to 24.8 wt.% (average = 11.5 wt.%) (Figures 7(b) and 8(a–h)), well in excess of typical

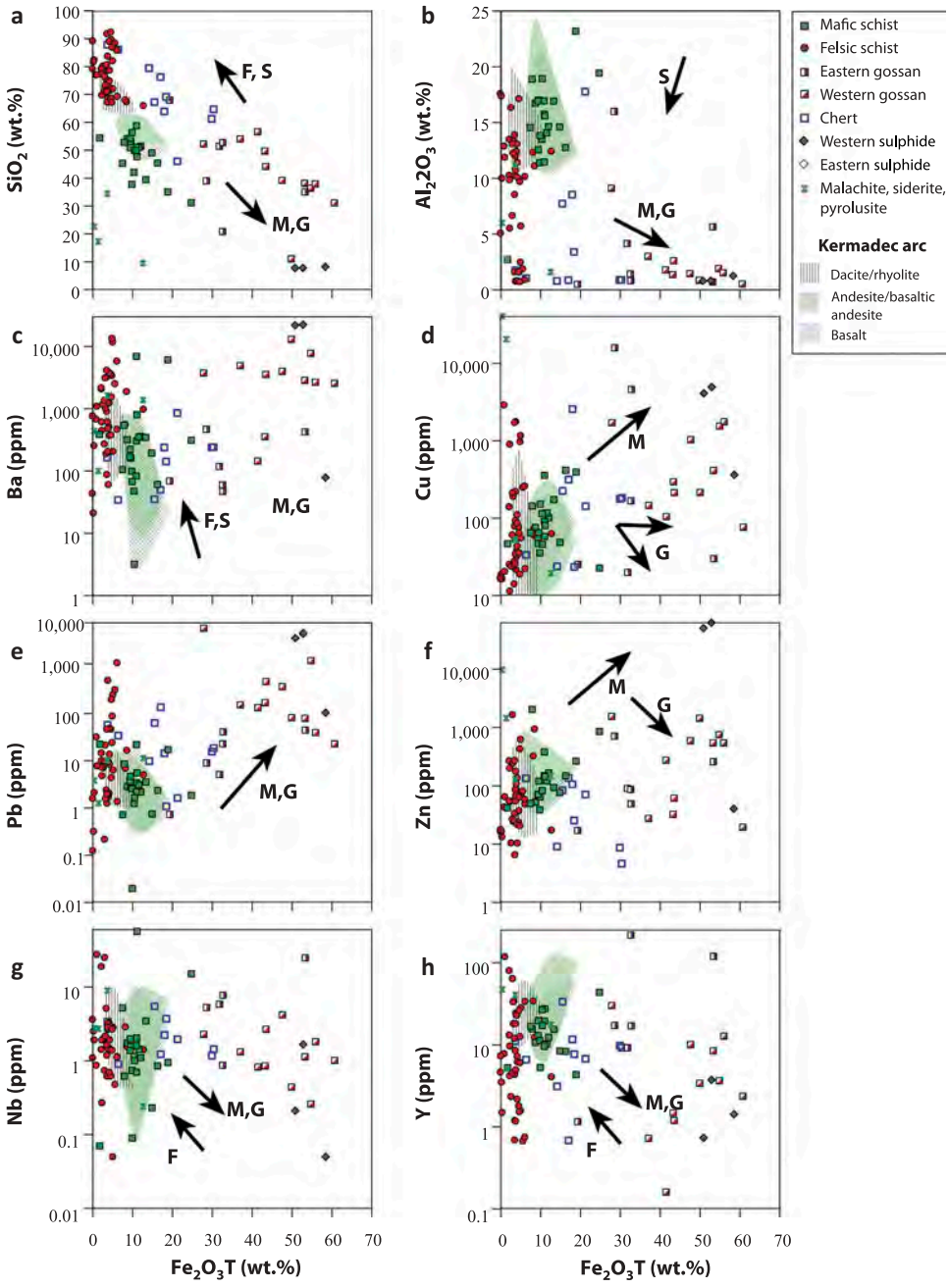

Figure 8. Bivariate plots of major and trace elements *versus* $Fe_2O_3^T$ content. The $Fe_2O_3^T$ content is a measure of igneous fractionation and addition of hydrothermal Fe during hydrothermal alteration and gossanization. (a) SiO_2 *versus* $Fe_2O_3^T$; (b) Al_2O_3 *versus* Zr; (c) Ba *versus* $Fe_2O_3^T$; (d) Cu *versus* $Fe_2O_3^T$; (e) Pb *versus* $Fe_2O_3^T$; (f) Zn *versus* $Fe_2O_3^T$; (g) Nb *versus* $Fe_2O_3^T$; (h) Y *versus* $Fe_2O_3^T$. Data from Supplementary Table 4. Also shown are fields for basalts, basaltic-andesite/andesite and dacite/rhyolite from the Kermadec arc (data from Wysoczanski, unpublished). General trends for crystal fractionation (F), silicification (S), gossanization (G), and massive sulphide mineralization (M) are also shown.

values for even the most Fe-rich least altered mafic volcanic rocks. Barium is much less variable and enriched compared to the felsic schists, ranging from 3.1 to 9000 ppm (average = 1300 ppm) (Figures 7(d) and 8(c)), but have on average higher Sr contents (30–925 ppm, average = 256 ppm; plot not shown). Chromium (Figure 7(e)) and Ni (not shown) are generally typical for moderately evolved basalts, ranging from 4 to 592 ppm (average = 114 ppm) and 8.5–263 ppm (average = 58 ppm), respectively. The HFSE have variable abundances in the mafic schists, but are remarkably similar to the felsic schists (Figures 7(a–h), 8(g–h), and 10(a–e)), and the lowest contents of the HFSE occur in carbonatized mafic schists. For all

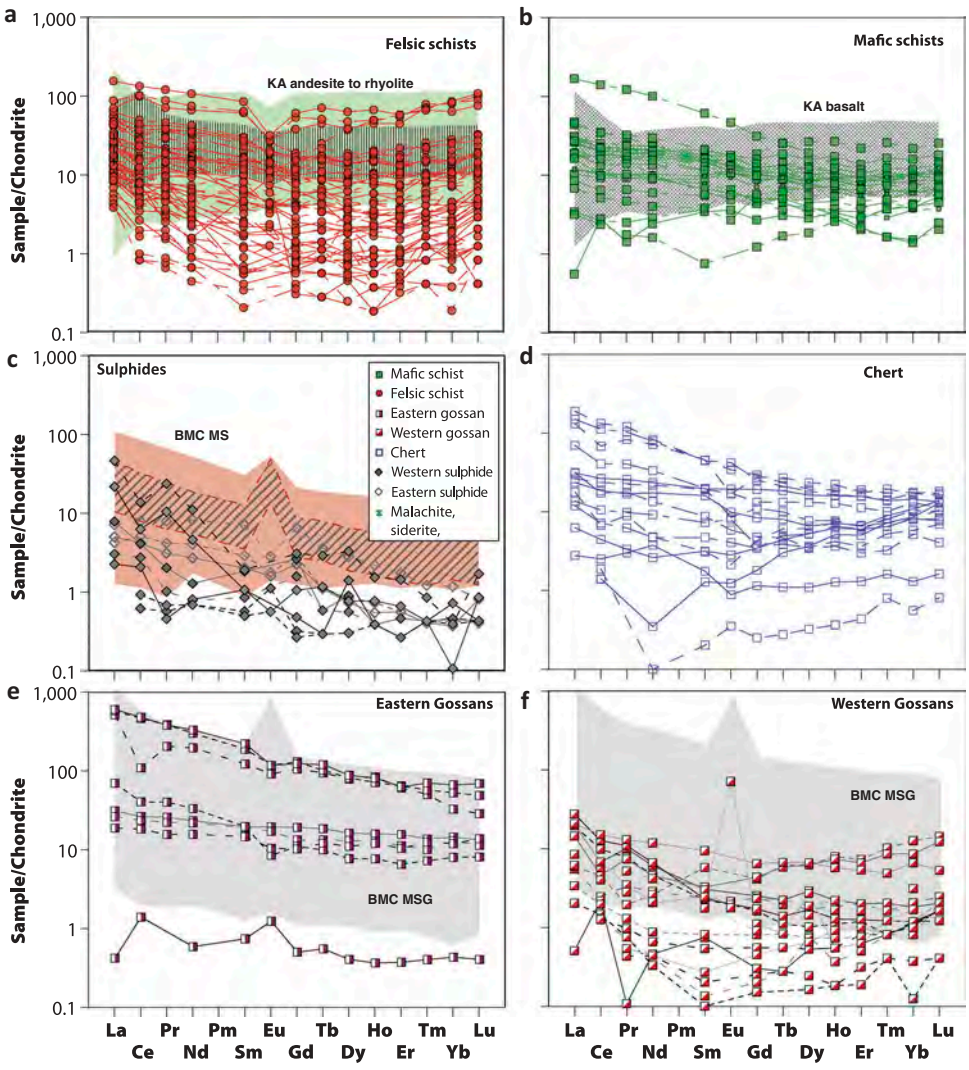

Figure 9. Chondrite-normalized rare earth element plots for the different sample types: (a) felsic schists (note the concave-up REE patterns for many of the samples); (b) mafic schists; (c) massive sulphides; (d) chert samples; (e) eastern gossans; and (f) western gossans. Normalizing values are from McDonough and Sun (1995). Data from Supplementary Table 4. Also shown are fields for basalts, basaltic-andesite/andesite and dacite/rhyolite from the Kermadec arc (data from Wysoczanski, unpublished). Gossan (massive sulphide gossan; MSG) data from the Bathurst Mining Camp (BMC) from Boyle (2003) and Leybourne *et al.* (2006). Massive sulphide (MS) data from the BMC are from (Goodfellow *et al.* 2003).

mafic schists, Zr ranges from 1.13 to 466 ppm (average = 50 ppm; Figure 7(g)), Y ranges from 3.2 to 43 ppm (average = 13.7 ppm; Figure 7(h)), Nb ranges from 0.07 to 56.7 ppm (average 4 ppm; Figure 8(g)) and Th ranges from 0.02 to 4.03 ppm (average = 0.8 ppm; plot not shown). The VMS-associated metals are variable in the mafic schists, with lower Cu and Pb contents than the felsic schists. Copper ranges from 22.6 to 410 ppm (average = 119 ppm; Figures 7(f) and 8(d)), Zn from 38 to 2005 ppm (average = 226 ppm; Figure 8(f)) and Pb from <1 to 25.5 ppm (average 5.64 ppm; Figure 8(e)).

The least altered mafic schists have generally flat to slightly LREE-enriched profiles that are remarkably similar to the less altered felsic schists (Figure 9(b)), i.e. mean ΣREE = 45 *versus* 42 ppm $[La/Sm]_{cn}$ = 2.1 *versus* 2.7, and $[La/Yb]_{cn}$ = 4.0 *versus* 3.9, respectively. The Eu anomalies (Eu/Eu*) range from 0.60 to 1.59 (average = 1.04) and Ce anomalies (Ce/Ce*) from 0.47 to 3.19 (average = 1.35). Most of the mafic schist samples have chondrite-normalized LREE > MREE > HREE, so that most lack the concave-up REE pattern that is common for the felsic schists (Figure 9). The mafic schists are characterized by generally low Ba/Eu (Figure 10(a, c)), and lower $[La/Sm]_{cn}$ (Figure 10(b)), $[Ba/Nb]_{pm}$ (Figure 10(d)), and Nb/Yb (Figure 10(e)) than the felsic schists. $[La/Nb]_{pm}$ values overlap those of the felsic schists and modern arc tholeiites (Figure 10(d)). On a primitive mantle-normalized trace element plot, the

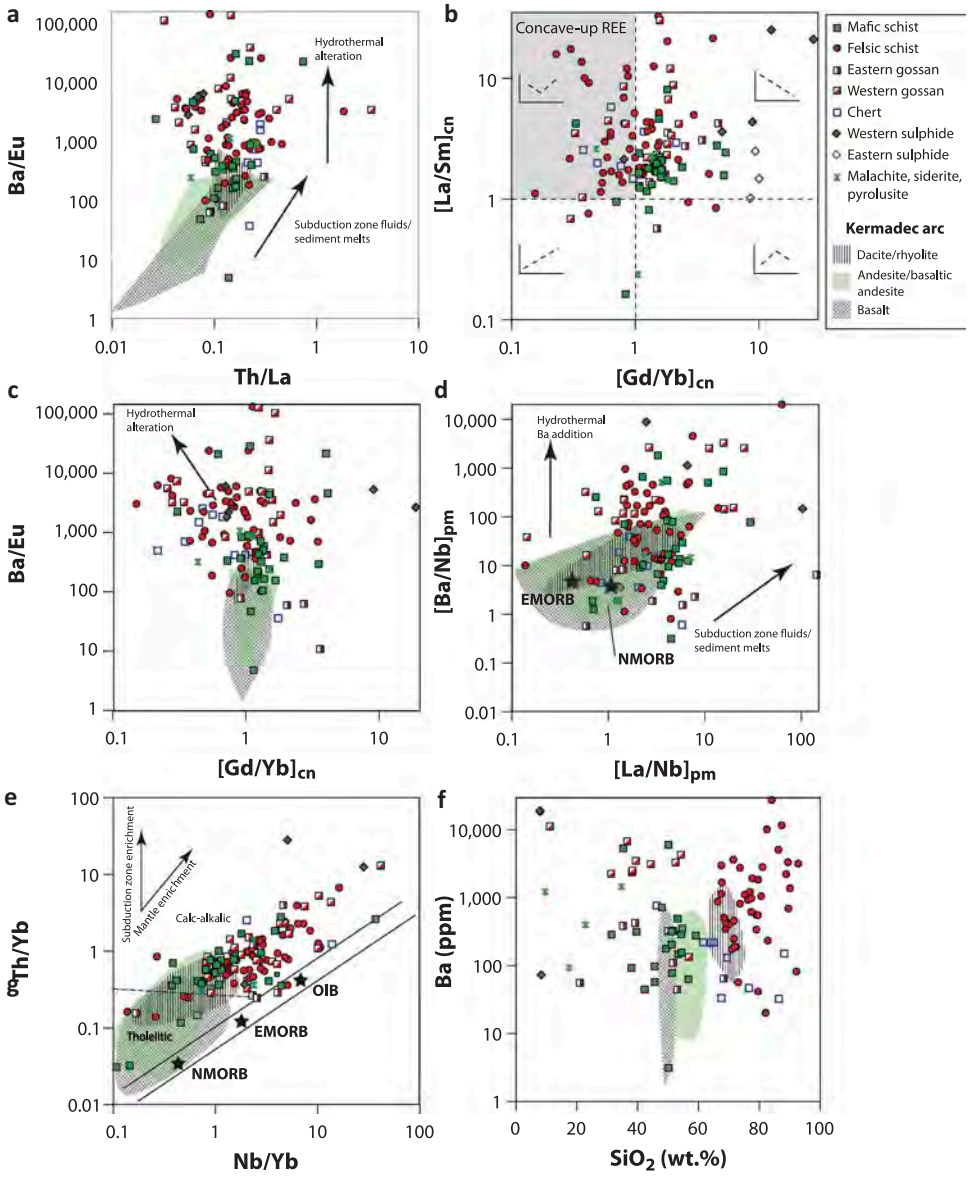

Figure 10. Bivariate plots of various trace and rare earth element ratios *versus* other trace and rare earth element ratios and SiO_2 *versus* Ba: (a) Ba/Eu *versus* Th/La. Addition of LILE by subduction zone fluids/subduction sediment melts will result in increasing Ba/Eu and Th/La, whereas addition of Ba by hydrothermal alteration will result only in relative increases in Ba/Eu; (b) $[La/Sm]_{cn}$ *versus* $[Gd/Yb]_{cn}$. Schematic in each quadrant of the diagram presents the simplified REE pattern. Only the felsic schists plot in the quadrant representing concave-up REE patterns; (c) Ba/Eu *versus* $[Gd/Yb]_{cn}$. (d) $[Ba/Nb]_{pm}$ *versus* $[La/Nb]_{cn}$. Values for NMORB and EMORB taken from the recent compilation of Gale *et al.* (2013); (e) Th/Yb *versus* Nb/Yb. Increasing influence from subduction zone fluids would increase the Th/Yb ratio, whereas mantle enrichment would cause a positive slope shift to higher ratios in both Th/Yb and Nb/Yb; (f) Ba *versus* SiO_2. Data from Supplementary Table 4. Also shown are fields for basalt, basaltic–andesite/andesite and dacite/rhyolite from the Kermadec arc (data from Wysoczanski, unpublished).

mafic schists display negative Nb anomalies, and moderate enrichment in Ba and Pb compared to adjacent elements (Figure 11(b)).

Cherts

The cherts are dominated by quartz (Supplementary Table 3), with SiO_2 contents that range from 46.1 to 87.9 wt.% (average = 70.3 wt. %; Figures 7(a) and 8(a)). The $Fe_2O_3^T$ contents range from 3.81 to 30.4 wt.% (average = 17.56), typically higher than the mafic and felsic schists (Figures 7(b) and 8(a–h)) and approaching values for ANS banded iron formations (Stern *et al.* 2013). Barium ranges from 32 to 758 ppm (average = 200; Figures 7(d) and 8(c)), and the cherts have variable Sr contents (17.5–339 ppm, average = 93; plot not shown); average Sr and Ba contents are lower than for the mafic schists. The HFSE abundances are variable

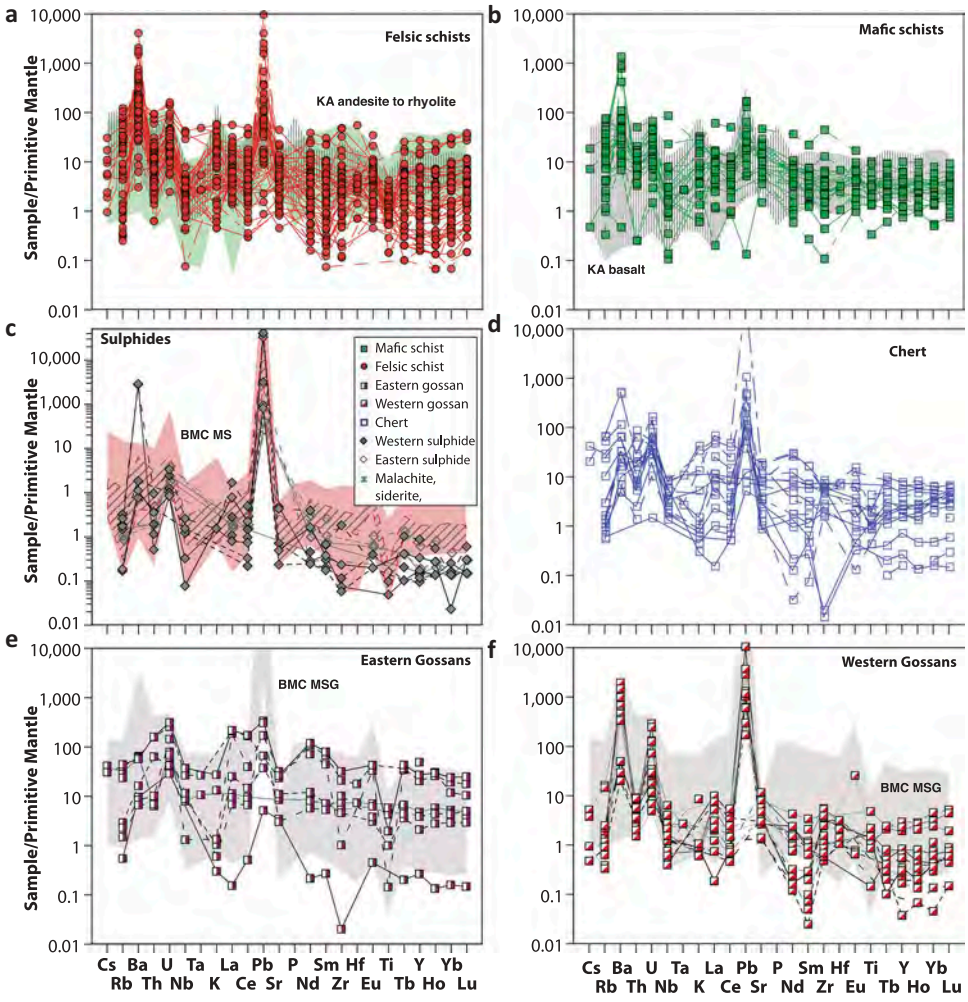

Figure 11. Primitive-mantle normalized spider diagrams for the different sample types: (a) felsic schists; (b) mafic schists; (c) massive sulphides; (d) chert; (e) eastern gossans; and (f) western gossans. Most of the mafic and felsic schists have Nb < La relative to primitive mantle. Normalizing values from McDonough and Sun (1995). Data from Supplementary Table 4. Also shown are fields for basalts, basaltic-andesite/andesite and dacite/rhyolite from the Kermadec arc (data from Wysoczanski, unpublished). Gossan (massive sulphide gossan; MSG) data from the Bathurst Mining Camp (BMC) from Boyle (2003) and Leybourne *et al.* (2006). Massive sulphide (MS) data from the BMC are from Goodfellow *et al.* (2003).

but are similar to both the felsic and mafic schists. For all cherts Zr ranges from 0.5 to 88.9 ppm (average = 40.1 ppm; Figure 7(g)), Y ranges from 0.68 to 33.2 ppm (average = 9.9 ppm; Figure 7(h)), Nb ranges from 0.9 to 5.48 ppm (average 2.4 ppm; Figure 7(g)) and Th ranges from 0.11 to 6.90 ppm (average = 1.43 ppm; not shown). The VMS-associated metal contents are variable, though lower than in the gossans (Figure 8(d, e), respectively). Copper ranges from 23 to 2520 ppm (average = 369 ppm; Figure 8(d)), Zn from 4.6 to 135 ppm (average = 60.3 ppm; Figure 8(f)), and Pb from 1.2 to 151 ppm (average 40.7 ppm; Figure 8(e)).

The cherts have generally flat to slightly LREE-enriched profiles (Figure 9(d)) that are similar to the schists with $[La/Sm]_{cn}$ = 1.47–5.76 (average = 2.7; Figure 9(b)), $[La/Yb]_{cn}$ = 0.77–7.71 (average = 3.1; plot not shown) and $[Gd/Yb]_{cn}$ = 0.21 to 1.60 (average = 0.68; Figure 9(b,c)). Eu anomalies are modest, with Eu/Eu* ranging from 0.48 to 1.54 (average = 0.85). The cherts have significant negative Ce anomalies (Ce/Ce*) from 0.54 to 0.98 (average = 0.81). The cherts are characterized by Ba/Eu (Figure 10(a,c)), $[La/Sm]_{cn}$ (Figure 10(a,b)), and Nb/Yb values (Figure 10(e)) that are similar to the felsic schists, although the felsic schists have higher values overall. Like the felsic schists, the cherts commonly have $[Gd/Yb]_{cn}$ <1 (Figure 10(b)). On a primitive mantle-normalized trace element plot, the cherts display negative Nb anomalies, moderate enrichments in Ba and U and significant enrichment in Pb compared to adjacent elements (Figure 11(d)).

Massive sulphides

The massive sulphides from both deposits contain widely ranging (but generally high) Cu, Zn, Pb, and Ba contents. Cu contents range from 360 to 15,575 ppm (average = 5465 ppm; Figures 7(f) and 8(d)), Zn ranges from 40 to 76,000 ppm (average = 26,000 ppm; Figure 8(f)), Pb contents range 40–6046 ppm Pb (average = 1973 ppm; Figure 8(e)), and Ba ranges from 50 to 18,794 ppm (average = 7484 ppm; Figure 8(c)), although Ba was not analysed in several samples (annex). The SAT (proximal) massive sulphide samples have higher Zn and Pb contents than those from Rabathan (distal) (with the exception of sample CO-13–84.15, which is pyrite-rich but low in Cu, Zn, and Pb; Figures 7(f) and 8(d–f)). In contrast, the massive sulphides at Rabathan have higher Cu contents (2310–17,575 ppm) than SAT.

The massive sulphides have low abundances of the HFSE and REE, consistent with low SiO_2 contents (<10 wt.%, although not all samples have major element analyses). The massive sulphide samples are characterized by REE profiles (Figure 9(e)) that are generally more LREE-enriched than the host schists, with $[La/Yb]_{cn}$ ranging from 3.2 to 256 (average = 56; plot not shown), and two samples have $[Gd/Yb]_{cn}$ <1 (Figure 10(b,c)). The sulphide samples from the Rabathan deposit have negative Eu anomalies (Eu/Eu* = 0.43–0.79; note that there are no Ba analyses), whereas the SAT sulphides analysed at ALS display positive Eu anomalies (Eu/Eu* = 1.55 and 2.64).

Gossans

The gossans have highly variable major element compositions, with SiO_2 contents ranging from 11.03 to 68.05 wt.% (average = 42.2 wt.%; Figure 7(a)) and $Fe_2O_3^T$ contents ranging from 19.4 to 60.7 wt.% (average = 42.0 wt.%; Figure 8(a–h)), consistent with a mineral assemblage dominated by goethite, haematite, quartz, and lesser jarosite minerals (Supplementary Table 3). Some of the gossans have high CaO and LOI (up to 20 wt.%), consistent with the presence of abundant calcite, as identified by XRD and in thin section. Barium is typically high compared to least altered rocks, as in the massive sulphides, ranging from 44.2 to 13,050 ppm (average = 2915 ppm; Figure 8(c)), whereas Sr and Rb contents are lower (Sr 26.3–642 ppm, average = 171 ppm; Rb 0.2–39.8 ppm, average = 7.3 ppm; plots not shown). The HFSE abundances are variable but are similar to those in the felsic and mafic schists. For all gossans, Zr ranges from 0.21 to 340 ppm (average = 50 ppm; Figure 7(h)), Y ranges from 0.16 to 214 ppm (average = 22.5 ppm; Figure 7(h)), Nb ranges from 0.26 to 24.8 ppm (average 3.54 ppm; Figure 7(g)) and Th ranges from 0.12 to 13.0 ppm (average = 1.66 ppm; plot not shown). The VMS-associated metals are variable (Figures 7(f) and 8(d–f)) with Cu ranging from 19.9 to 15,460 ppm (average = 1624 ppm; Figures 7(f) and 8(d)), Zn from 17.0 to 1524 ppm (average = 409 ppm; Figure 8(f)) and Pb from 0.78 to 7645 ppm (average 657 ppm; Figure 8(e)), but are noticeably lower in most cases, as expected, than values in the massive sulphide.

The gossans have generally flat to LREE-enriched profiles (Figure 9(f)), and they are similar to more LREE-enriched than the schists with $[La/Sm]_{cn}$ = 0.57–29.97 (average = 4.8; Figure 10(b)), $[La/Yb]_{cn}$ = 0.45–23.24 (average = 7.24; plot not shown) and $[Gd/Yb]_{cn}$ = 0.25–3.25 (average = 1.1; Figure 9(b,c)). Several gossans have concave-up REE patterns like the more altered felsic schists (Figures 9(f) and 10(b)). The high Ba contents in most gossans precluded calculation of Eu anomalies in UTD analyses where Ba/Eu >2000, but Eu anomalies could be calculated for all ALS analyses. The Eu anomalies (Eu/Eu*) vary widely range from 0.58 to 91.6 (average = 8.55) and Ce anomalies (Ce/Ce*) from 0.34 to 9.29 (average = 1.22). The incompatible element ratios and primitive-mantle normalized profiles for the gossans are similar to the felsic schists and massive sulphides, with enrichments in Ba, U, and Pb (Figures 10 and 11).

Discussion

The field, mineralogical, and geochemical data presented above allow new insights on the following five topics: (1) geochemistry and tectonic setting of mafic and felsic schists; (2) the origin of the SAT deposit; (2) gossan formation; (4) rare earth element behaviour of gossanization; and (5) implications for mineral exploration. These are discussed in the following.

Geochemistry and tectonic setting of mafic and felsic schists

The WBMD has experienced three phases of deformation, and has been regionally metamorphosed to greenschist facies (Volesky *et al*. 2003; Sangster and Abdulhay 2005). Although igneous protoliths can be identified in some cases, for the most part the country rocks are too strongly deformed for confident identification. Mafic and felsic schists were likely deposited as flows and tuffs. The more primitive character of the mafic schists compared to the felsic rocks is consistent with greater Cr and Ni (average = 122 and 62 ppm) compared to the felsic schists (average = 14 and 11 ppm; Figure 7(e)).

Compared to primitive mantle, the mafic and felsic schists, despite their degree of alteration, show some commonalities: Nb is typically depleted compared to the LREEs (e.g. La on Figures 11(a,b)), whereas both Ba and Pb are enriched compared to similarly incompatible elements. For example, most of the mafic schists have values of Ba/Eu (Figure 10(a)) and $[Ba/Nb]_{pm}$ (Figure 10(d)) similar to rocks from modern intra-oceanic arcs, such as the Kermadec arc. In contrast, the felsic schists show a trend to increasing Ba (Figure 10(a,c,d)) and Pb (plot not shown) with increasing alteration intensity, suggesting that Ba and Pb were added during hydrothermal alteration, likely during formation of the massive sulphide deposits. We compare WBMD rocks with rocks of the Kermadec arc because we interpret the most likely tectonic setting of the former as an oceanic arc (Figure 12(a,b)). Such a setting is also consistent with addition of Ba observed for the mafic schists; LILE are preferentially mobilized in subduction zone fluids, from altered oceanic crust and overlying sediments, enriching the mantle wedge (e.g. Th/Yb above the mantle array; Figure 10(e)).

Several samples mapped as felsic schists have high SiO_2 and low Zr (Figure 7(a)) and TiO_2 contents (plot not shown). Petrographically, these rocks are dominated by quartz, suggesting that these were either originally quartz-rich volcaniclastic or sedimentary rocks or were volcaniclastic rocks that were silicified

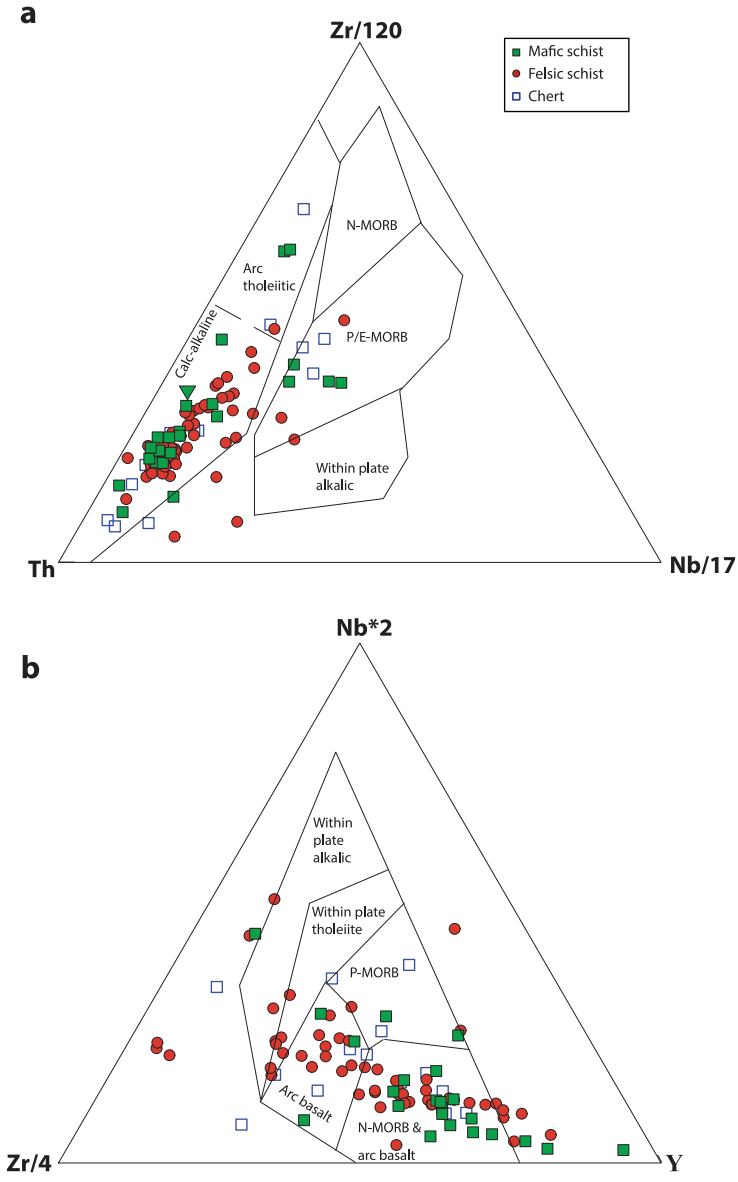

Figure 12. (a) Th–Zr/120–Nb/17 ternary discrimination plot for mafic volcanic rocks (as a proxy for Th–Hf/3–Ta as originally devised by Wood (1980)). (b) Zr/4–Nb*2-Y ternary discrimination diagram for mafic volcanic rocks (Meschede 1986). Data from Supplementary Table 4.

owing to higher porosity and permeability compared to the volcanic rocks, leading to a decrease (dilution) of Zr. Most of the felsic schists likely have a volcanic or volcanosedimentary precursor. Despite their high SiO_2 contents (>65 wt.%; Figure 7), the felsic schists, which fall in the dacite and rhyolite fields on a total alkali-silica diagram (not shown), plot as andesites on the Zr/TiO_2 *versus* Nb/Y plot used for highly altered rocks (Figure 5(a)) (Winchester and Floyd 1977). There are two possible explanations for this disparity: (1) the felsic schists represent anatexis of mafic crust in an oceanic environment, in the presence of residual amphibole; or (2) the felsic schists represent silicified equivalents of the mafic schists, albeit slightly more evolved (i.e. higher Zr/TiO_2). The first explanation is based on the work of Brophy (2008) who showed that there is little fractionation in REE contents relative to SiO_2 during partial melting of oceanic crust in the presence of amphibole. In contrast, where more silicic rocks are produced by crystal fractionation in the absence of amphibole, REE contents increase with increasing SiO_2 content (Brophy 2008). Additional evidence from the felsic and mafic schists supports this explanation. The felsic and mafic schists show similar ranges in REE (e.g. La, Yb) and HFSE (e.g. Nb, Zr, and Y) contents (Figure 7(g)) suggesting that they are not related by extensive crystal fractionation.

Another distinguishing feature of many of the felsic schists (and cherts and gossans) are their concave-up REE patterns (Figure 9(a)) (i.e. many felsic schists have $[La/Sm]_{cn}$ >1 with $[Gd/Yb]_{cn}$ <1 (Figure 10(b))). Concave-up REE patterns are uncommon in volcanic rocks and generally only occur in boninites that are generally restricted to fore-arc environments (Stern and Bloomer 1992). However, concave-up REE patterns are now recognized in felsic volcanic rocks influenced by either residual amphibole during partial melting or fractionation of amphibole during crystallization and in hydrothermally altered felsic volcanic rocks (Barrie *et al*. 2007).

The felsic schists trend to much higher Ba (Figure 8(b)) and Pb (Figure 8(e)) contents than the mafic rocks, most likely due to addition during hydrothermal alteration; some degree of silicification is therefore also likely (Gibson *et al*. 1983; Sharpe and Gemmell 2001; Peter *et al*. 2014), which would dilute the REE and HFSE contents, perhaps bringing them down to levels similar to the mafic schists (Figures 7 and 8). Further, other studies have suggested that concave-up REE patterns in felsic rocks associated with VMS deposits may be imparted by hydrothermal alteration (Barrie *et al*. 2007). The felsic schists and gossans have REE patterns that are significantly more concave-up than do most of the mafic schists (Figure 10(b); $[Gd/Yb]_{cn}$ <1 and $[La/Sm]_{cn}$ >1).

The felsic schists likely are rhyolites and andesites (and their volcaniclastic equivalents) produced by partial melting of mafic lower crust in the presence of amphibole, and were subsequently hydrothermally altered. The volcanic sequence (rock types and stratigraphic relationships) of the Wadi Bidah area, together with the trace element geochemical characteristics of the rocks are consistent with deposition in an oceanic arc tectonic setting (Figures 10(d,e), 12, and 13(a)). This interpretation would explain the similarity in REE and HFSE abundances despite large differences in SiO_2 contents (Brophy 2008), and also the Zr/TiO_2 values that are not sufficiently fractionated to classify the felsic schists as dacites or rhyolites that were silicificed. Elevated Ba, base metals and SiO_2 contents are interpreted to be due to addition by hydrothermal fluids that circulated through the rocks to form the massive sulphides. We interpret the hydrothermally altered schists to reflect interaction with the high-temperature hydrothermal fluids that formed the massive sulphide deposits and precipitated disseminated sulphides in the subsurface.

The SAT deposit

Typical volcanogenic massive sulphide deposits consist of a stratiform lens of massive sulphide and a discordant zone of stockwork mineralization within hydrothermally altered rocks of the stratigraphic footwall (Galley *et al*. 2007). The hydrothermal alteration at SAT is manifested by iron-, clay-, chlorite-, and calcite-enriched zones (Coumoul *et al*. 1989). The SAT deposit is stratabound and hosted within a steeply dipping chloritic schist unit (Figure 3). Coumoul *et al*. (1989) indicated that the SAT deposit has a large-scale epidote–chlorite–carbonate alteration zone to the west of a quartz–sericite–pyrite zone and an asymmetric, small scale, quartz–kaolinite–alunite–chlorite zone surrounding the epidote–chlorite–carbonate zone. The SAT quartz–sericite–pyrite zone is interpreted as the envelope of a feeder pipe to a hydrothermal vent (Coumoul *et al*. 1989).

The present water table at SAT lies 45 m below the surface (Figure 3). Below the water table, stratiform layers of massive sulphide within steeply dipping felsic schist characterize the deposit. The gossan that formed above the water table is the up-dip equivalent of the massive sulphide and consists of haematite, goethite, quartz, jarosite group minerals, calcite and barite (Supplementary Table 3; Figure 3). We suggest that the lithological variation with respect to the SAT water table reflects supergene weathering of the massive

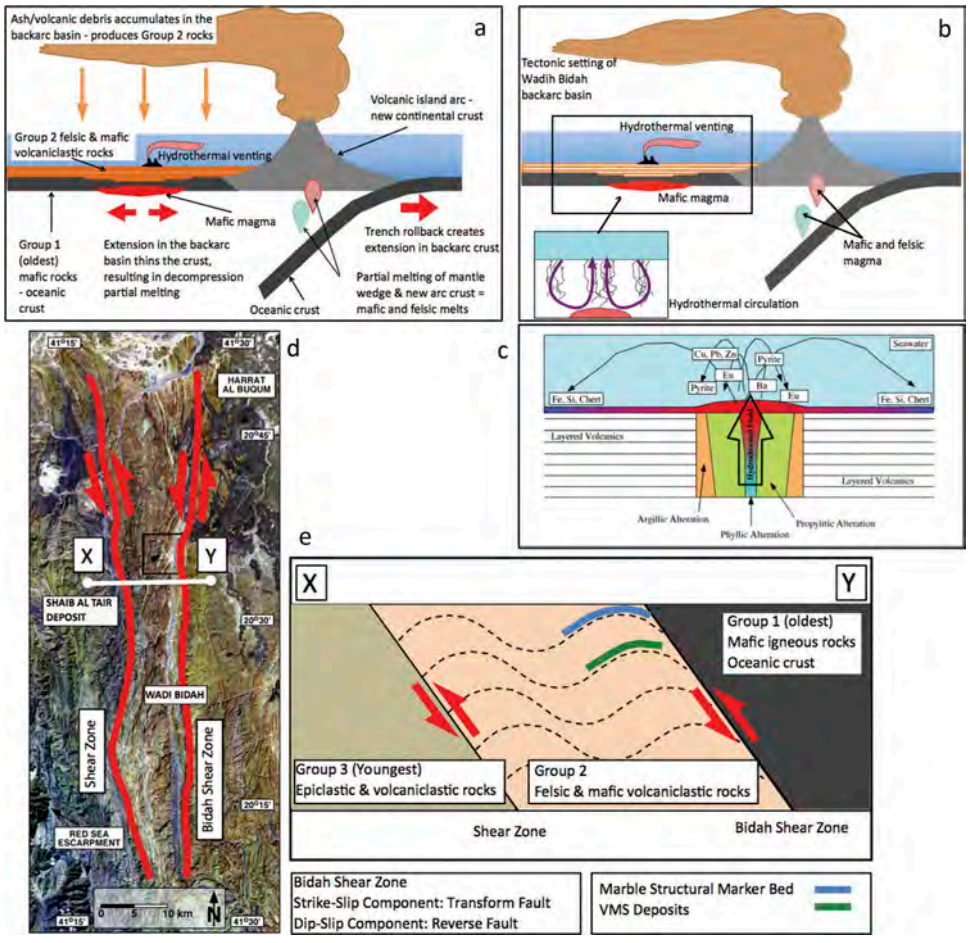

Figure 13. Model for the development of the Wadi Bidah mineral belt and SAT and Rabathan deposits. (a) and (b) Formation of sea floor massive sulphide deposits and group 1–3 rocks in an arc/back-arc basin setting associated with Neoproterozoic subduction; (c) Schematic representation of formation of sulphide mounds, chemical sediments and associated hydrothermal alteration; (d and e) Structural evolution along the Wadi Bidah.

sulphides as a result of a fluctuating Quaternary water table, which is likely now falling in the arid environment of modern Saudi Arabia (Figure 13). We therefore classify the SAT gossan as a massive sulphide gossan (Boyle 2003). This interpretation is consistent with its mineralogy and geochemistry.

Volcanogenic massive sulphide formation

Volcanogenic massive sulphide deposits, such as those in the WBMD, form in submarine environments by precipitating sulphides from a quenched hydrothermal fluid upon mixing with cold seawater (Solomon and Walshe 1979; Galley *et al*. 2007). The hydrothermal fluids are modified seawater that has been heated and chemically modified by reaction with hot rocks a few tens to hundreds of metres below the seafloor, in a high-temperature reaction zone, with variable contributions from magmatic volatiles (Gemmell *et al*. 2004; De Ronde *et al*. 2011). Studies of hydrothermal fluids at mid-ocean ridge and back-arc basin spreading centres indicate that convecting seawater becomes heated, reduced, and acidic due to interaction with volcanic and intrusive rocks in the subsurface (Beaudoin and Scott 2009). High-temperature hydrothermal fluids (>250°C) are preferentially enriched in Eu relative to other REE due to crystochemical exchange with plagioclase (Klinkhammer *et al*. 1994); the Eu mobilized by the upwelling hydrothermal fluids is deposited in the massive sulphide and exhalite precipitates (Sverjensky 1984; Leybourne *et al*. 2006). Low-temperature (<250°C) hydrothermal fluids do not generally have positive Eu anomalies (Michard 1989). Although both ancient and modern volcanogenic massive sulphide deposits have extremely variable REE contents, they are generally much richer in REE than modern vent fluids, indicating that the REE are trapped during precipitation of the base metal sulphides (Gieré 1993; Peter *et al*. 2003). The REE are not incorporated into the sulphide minerals (Morgan and Wandless 1980), but rather in minor

phases (i.e. monazite, Y-, Ce-, or Nd-aeschynite, zirconolite [$CaZrTi_2O_7$]/zirkelite [$(Ca,Th,Ce)Zr(Ti,Nb)_2O_7$], apatite, allanite, titanite, barite, and anhydrite) with a high affinity for REE (Gieré 1993; Pan *et al*. 1994; Peter *et al*. 2003; Genna *et al*. 2014a). The REE pattern of massive sulphides precipitated at the vent and chemical sediments (exhalites) precipitated at some distance around it typically reflect the REE pattern of the hydrothermal solution (Graf 1977). Recent studies of the seafloor sediments surrounding the modern day Pacmanus volcanic hosted massive sulphide field in the Eastern Manus Basin show that the Eu/Eu* is particularly useful in discriminating proximal from distal deposits with respect to the main hydrothermal vent. Positive Eu anomalies are also characteristic of ancient volcanogenic massive sulphide deposits (Peter *et al*. 2003; Leybourne *et al*. 2006) and many Archaean banded iron formations (Derry and Jacobsen 1990; Kato *et al*. 2006; Sugahara *et al*. 2010).

Gossan formation

Weathering processes acting on massive sulphides (i.e. supergene weathering or gossanization) are important because they enrich precious and base metals in the supergene enriched zone below the gossan to such a degree that even low grade primary sulphides or precious metal-bearing mineralized zones can form economic mineral deposits (Boyle 1996). Gossanization results from the chemical interaction of oxygenated aqueous solutions (meteoric and groundwater) with sulphide minerals (Thornber and Taylor 1992). Supergene weathering throughout the Arabian Shield extends down to a depth of 30–40 m (Ryall and Taylor 1981). This type of supergene weathering is characteristic of gossan formation around the world (Cortial *et al*. 1985; Cottard *et al*. 1986; Marcoux *et al*. 1989; Boyle 1994, 2003; Barrie *et al*. 2007; Velasco *et al*. 2013).

Ryall and Taylor (1981) described Saudi Arabian gossans as a type of ironstone, forming the weathered surface expression of a rock originally dominated by sulphides. Blain (1977) and Taylor (1987) expanded gossan classification to include base metal sulphide gossans, iron sulphide gossans, and several types of transported gossans. Boyle (2003) refined the classification scheme for the glaciated Canadian environment, where many ironstones are displaced from their source and all ironstones are classified as gossans, with suitable prefixes given once a source has been verified by field, mineralogical, or geochemical techniques. Boyle (2003) identified six types of gossans in the vicinity of massive sulphide deposits: (1) massive sulphide gossans (MSG), formed *in situ* by weathering of primary sulphides; (2) ferruginized wall rock gossans, formed as a result of Fe-rich acidic groundwater flowing through hanging wall and footwall lithologies and adding Fe; (3) stockwork/disseminated zone gossans; (4) leached wall-rocks, resulting from leaching of deposit-hosting lithologies by acidic groundwaters resulting from gossanization and are dominantly quartz, kaolinite, and white mica (sericite); (5) mechanically transported gossans, transported by glacial or mass wasting processes; and (6) hydromorphically transported gossans, formed as the result of reprecipitation of Fe where mineralized groundwater exits into an oxidizing environment. On the basis of textures, mineralogy (e.g. Supplementary Table 3) and geochemistry, we interpret the WBMD gossan samples here to dominantly consist of massive sulphide gossans. These samples generally have high Fe_2O_{3T}, Cu, Zn, Pb, and Ba contents (all metals that commonly occur in VMS deposits (e.g. Zn–Pb–Cu massive sulphides and massive sulphide gossans from the Bathurst Mining Camp; Figure 8(c–f)) compared to host rocks and have REE profiles similar to the massive sulphide samples (Figure 9(e,f)). The WBMD gossans are dominantly composed of haematite, goethite, and quartz. These gossans also have jarosite group minerals (jarosite and natrojarosite), minerals that form only under low pH (<3), oxidizing conditions (Boyle 2003). The apparent absence of alunite implies that Fe/Al »1 (molar) and the presence of jarosite and natrojarosite implies that during gossan formation, the proportions of K and Na available were variable. There is no geochemical evidence that any of the gossans sampled are hydromorphic gossans; these typically are enriched in Zn, the most mobile of the VMS-associated metals. The WBMD gossans as a whole show depletion in VMS metals in the order Zn > Cu > Pb. Lead is typically the least mobile of these metals during gossan formation and is incorporated into jarosite minerals (including plumbojarosite if sufficiently abundant) at low pH, or anglesite and cerussite at progressively higher pH (Boyle 2003; Leybourne *et al*. 2006; Velasco *et al*. 2013). Copper is mobile under acidic oxidizing conditions, but is typically precipitated below the water table, increasing Cu contents of Cu-sulphide minerals (Boyle 2003). The high Cu contents of some chert and altered felsic schist samples likely reflect Cu precipitated from gossan-forming groundwaters. Zinc is mobile under the acidic oxidizing conditions inferred to form WBMD gossans. Although S contents are typically low in such gossans (e.g. WMBD gossans have S of 0.06 to 0.28 wt.% compared to ~50 wt.% in massive sulphides (Leybourne and Volesky, unpublished data), S is partially retained as SO_4 in the jarosite minerals. Enrichment of Pb compared to Cu and Zn is

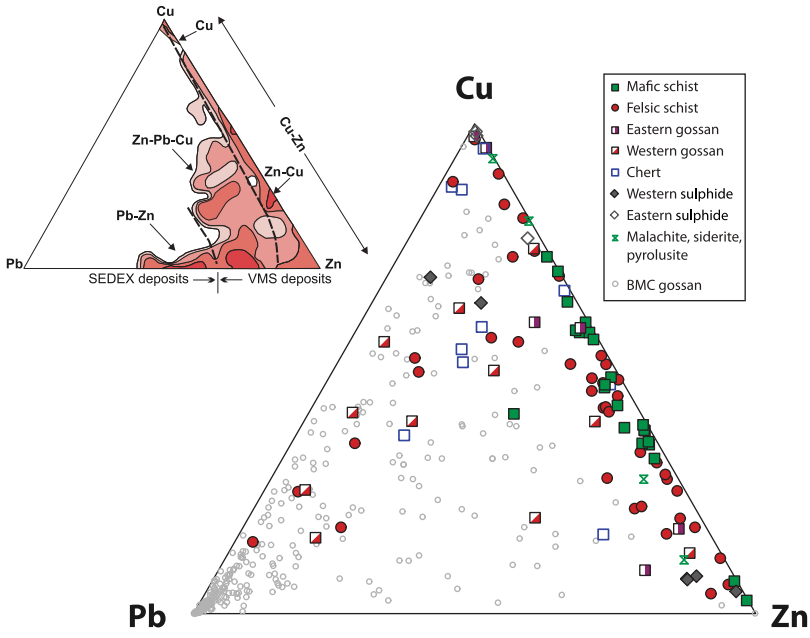

Figure 14. Ternary plot of Pb–Cu–Zn for all samples from this study. Also plotted are massive-sulphide gossan samples from the Bathurst Mining Camp (Boyle 2003). Inset shows same plot for world VMS deposits (Galley *et al*. 2007). Gossanization generally causes samples to lie closer to the Pb apex and further away from the Zn apex; this is because Zn is mobile, Pb relatively immobile, and Cu typically is removed from the oxidizing portion and reprecipitated as enriched Cu-sulphides below the water table (Boyle 2003). Data from Supplementary Table 4.

demonstrated on a ternary diagram of Pb–Cu–Zn (Figure 14). Primary massive sulphides from oceanic settings fall along the Cu–Zn join, whereas those from continental settings, such as the Bathurst Mining Camp (BMC), tend to fall along the Zn–Pb join (except Cu-rich stockwork zones; Boyle 2003). Gossan samples from the WBMD and those from the BMC are more Pb-rich relative to Cu and Pb compared to precursor massive sulphides (Figure 14).

The textures, mineralogy and geochemistry of WBMD cherts suggest that they may in part represent leached wall-rock gossans. The cherts are characterized by Cu, Pb, and Zn contents that are higher than the felsic schists, with concomitantly high $Fe_2O_3^T$ contents (Figure 8(d–f)), suggesting that these rocks have been altered as a result of acidic groundwaters generated during gossan formation. These acidic fluids would have been enriched in Cu, Pb, Zn, and Fe, with precipitation of these metals as alteration progressed. This alteration likely also resulted in intense silicification of these rocks, as well as the felsic schists. Alternatively, the cherts may be hydrothermal chemical sediments that extend along-strike from the massive sulphides, similar to metalliferous sediments in modern seafloor hydrothermal systems (Peter *et al*. 2003) or formed by the silicification of porous units (Galley *et al*. 1995; Genna *et al*. 2014b). The cherts occupy the same stratigraphic horizon as the gossans. If the cherts are exhalites that are lateral equivalents to massive sulphides, the general lack of positive Eu anomalies is consistent with increasing influence of the hydrothermal fluid with proximity to the vent upflow zone, as seen elsewhere, or these chemical sediments were precipitated at lower temperature («250°C). Some of the cherts have high Cu, Zn, and Pb contents, consistent with an exhalative origin, although Zr contents (<20–90 ppm) indicate variable mixing with clastic detrital sediments.

Gossanization and REEs

The two most important factors controlling the solubility and mobility of an element during gossanization are oxidation potential (Eh) and hydrogen ion activity (pH) (Thornber and Taylor 1992). The REE (including redox sensitive Ce^{3+}/Ce^{4+} and Eu^{3+}/Eu^{2+}) data can therefore be used to constrain conditions of gossan formation (climate, Eh, pH, salinity, temperature). It is widely recognized that REE are somewhat mobile on a microscopic scale during diagenesis and metamorphism (Kuschel and Smith 1992; Hodder 1994), but on a larger scale (hand-sample) the REE are immobile in most cases and for this reason are commonly used as indicators of protolith composition (Haas *et al*. 1995). The preservation of the REE profiles and positive Eu anomalies

during gossanization has previously been documented for the massive sulphide deposits in the BMC, New Brunswick, Canada (Leybourne *et al*. 2006). However, Pérez-López *et al*. (2010) investigated the REE composition of gossans and massive sulphide waste in the Iberian Pyrite Belt and found that during gossan formation the MREE were more mobile, resulting in concave-up REE patterns in the gossans, and this feature is not present in the massive sulphide tailings. The sulphide tailings also do not possess positive Eu anomalies; however, the genetic relationship between the sulphide tailings and the gossan they studied is unclear. The WBMD massive sulphides investigated here have flat to LREE-enriched chondrite normalized REE profiles, with rare samples showing concave-up REE patterns, and some showing positive Eu anomalies and variably negative and positive Ce anomalies (Figure 9(f)).

The REE profiles of the base metal-rich massive sulphide samples with positive Eu anomalies and negative Ce anomalies can be explained by reference to modern hydrothermal systems (Klinkhammer *et al*. 1994; Craddock *et al*. 2010). The preferential accommodation of Eu^{2+} in reducing environments and the dominance of Eu^{2+} at temperatures >250°C suggest that positive Eu anomalies in hydrothermal precipitates indicate precipitation from hot, reducing hydrothermal fluids, and that negative Eu anomalies imply Eu^{3+} dominance, reflecting more oxidizing conditions. Examples of modern seafloor massive sulphide deposits having positive Eu anomalies are known from modern mid-ocean ridges and in back-arc basins and oceanic arc settings (Barrett *et al*. 1990; Bau *et al*. 2010; Craddock *et al*. 2010). Similar REE patterns have also been recognized in ancient sulphide deposits and iron formations (Figure 9(c), BMC massive sulphides; Peter *et al*. 2003; Leybourne *et al*. 2006; Genna *et al*. 2014a). We suggest that the positive Eu anomaly in the metal-rich massive sulphide samples reflects the primary, high-temperature hydrothermal fluid, which formed the deposit. In contrast, the samples of massive sulphide with low metal contents and negative Eu anomalies may reflect earlier, lower temperature hydrothermal fluids or mixing with clastic detritus, which possessed negative Eu anomalies. Interestingly, the massive sulphides at Rabathan have negative Eu anomalies but are Cu-rich, which typically indicates higher temperatures (Crerar and Barnes 1976).

A simple model can be constructed to account for the geochemical characteristics of the SAT and Rabathan deposits: (1) low temperature hydrothermal processes produced the base metal- and Ba-poor massive pyrite lacking positive Eu anomalies; (2) precipitation from high-temperature hydrothermal fluids produced massive sulphide with enrichment of Ba, Pb, Zn, and Fe and, in some cases, the characteristic positive Eu anomaly and LREE-enrichment (the latter possibly enhanced by incorporation of LREE-enriched clastic detritus compared to chondrite); (3) WBMD massive sulphide deposits and host rocks underwent greenschist grade metamorphism and at least three neoproterozoic deformational events (Volesky *et al*. 2003); (4) subsequent uplift and erosion exposed the massive sulphides and host rocks to oxygenated meteoric waters; and (5) Supergene weathering altered the massive sulphide mineralogy under low pH (<3), highly oxidizing conditions concomitant with a falling water table (Figure 13). Despite intense supergene weathering, original REE profiles are preserved (Figure 9(e,f)), but Cu and Zn contents are lower in the oxidized zone or gossan compared to the primary sulphide, whereas Ba, Pb, and Fe contents in the gossan are similar to those in the massive sulphides (Figure 8(c,e,f)).

The timing of gossan formation in WBMD is uncertain, but geomorphologic considerations suggest processes spanning much of the Cenozoic. The WBMD has considerable relief, with dissection of the southern Arabian Shield accompanying rift-margin uplift associated with the opening of the Red Sea. Apatite and zircon (U–Th)/He thermochronometry (AHe and ZHe) on exhumed rocks in the northwestern and west-central parts of the Arabian Shield, detrital AHe thermochronometry on syn–rift sedimentary packages, whole-rock $^{40}Ar/^{39}Ar$ dating and X-ray fluorescence analyses of syn- and post-rift flood basalts, and numerical time-temperature modelling of AHe and ZHe systems reveal a three stage thermotectonic history for the central Arabian rift flank (CARF) along the eastern margin of the Red Sea (Szymanski 2012). The region underwent a pre-rift Palaeozoic–Mesozoic cooling event that brought the basement rocks to a mid-to-upper crustal structural level where they remained thermally stable through the Mesozoic. A major rift pulse ~23 Ma subsequently exhumed a 200 km-wide zone of the rift margin. Both the SAT and Rabathan gossans crop out close to the present-day base-level of Wadi Bidah, which because of ~23 Ma exhumation and uplift cuts deep into the Mesozoic and older erosion surface of relatively low relief that is preserved along the lip of the Red Sea Escarpment, a few hundred metres above the Wadi Bidah gossans. Therefore, the SAT and Rabathan gossanous weathering profiles developed since the primary sulphides were exposed to weathering because of Wadi Bidah down-cutting, and are therefore younger than ~23 Ma. Weathering and gossan formation continues to the present (Figure 13).

Implications for mineral exploration

The trace element geochemistry of volcanic rocks can be used to identify the geologic terranes and volcanic/volcanosedimentary belts favourable for hosting mineral deposits, and can be used to assess regional scale potential for mineral deposits (Kerrich and Wyman 1996; Piercey 2007, 2011). Using lithologic and geochemical criteria, Syme *et al*. (1996) were able to differentiate productive and barren volcanic sequences in the Flin Flon greenstone belt of Canada. This type of analysis can be used to focus exploration in particular volcanic assemblages within a greenstone belt. Immobile element data (e.g. HFSE, REE) can also be used to correlate stratigraphic units (Lentz 1996). The geochemical composition, particularly the trace elements, of volcanic host rocks can provide strong evidence of the regional to local tectonic setting of deposit formation (Lentz 1996). In many cases, there is a strong spatial relationship between volcanogenic massive sulphide deposits, regional-scale hydrothermal alteration zones and underlying subvolcanic intrusions (Galley *et al*. 2007). Major element lithogeochemical vectors based on whole-rock composition may serve to define vectors to ore by tracking the chemical and mineralogical changes associated with hydrothermal alteration (Large *et al*. 2001b). This may involve whole-rock data to distinguish igneous fractionation and volcanic component mixing trends from hydrothermal alteration associated with mineralization (Large *et al*. 2001b), and determining chemical changes associated with hydrothermal alteration in conjunction with immobile element chemostratigraphy (Barrett *et al*. 1991, 1999).

Peter *et al*. (2003) studied iron formations (exhalites) associated with volcanic hosted massive sulphide deposits in the Bathurst Mining Camp, New Brunswick, Canada to determine if bulk geochemical variations could be used to link iron formations and massive sulphides. Modern hydrothermal sediments display mineralogical and geochemical zonation around vent sites at the local and regional scale (Peter *et al*. 2003). The recognition of mineralogical zonation such as greater sulphide content, Fe, Mn, and base metal abundances in ancient iron formations may serve as a vector toward centres of palaeohydrothermal venting and massive sulphide mineralization (Peter *et al*. 2003).

We have herein documented relationships between massive sulphide formation, intensity of hydrothermal alteration, and overprinting gossanization and bulk rock geochemical composition that can be used to guide further exploration in Saudi Arabia and elsewhere in the ANS. For example, there is a strong positive relationship between metal contents (Cu, Zn, Pb), Ba, and

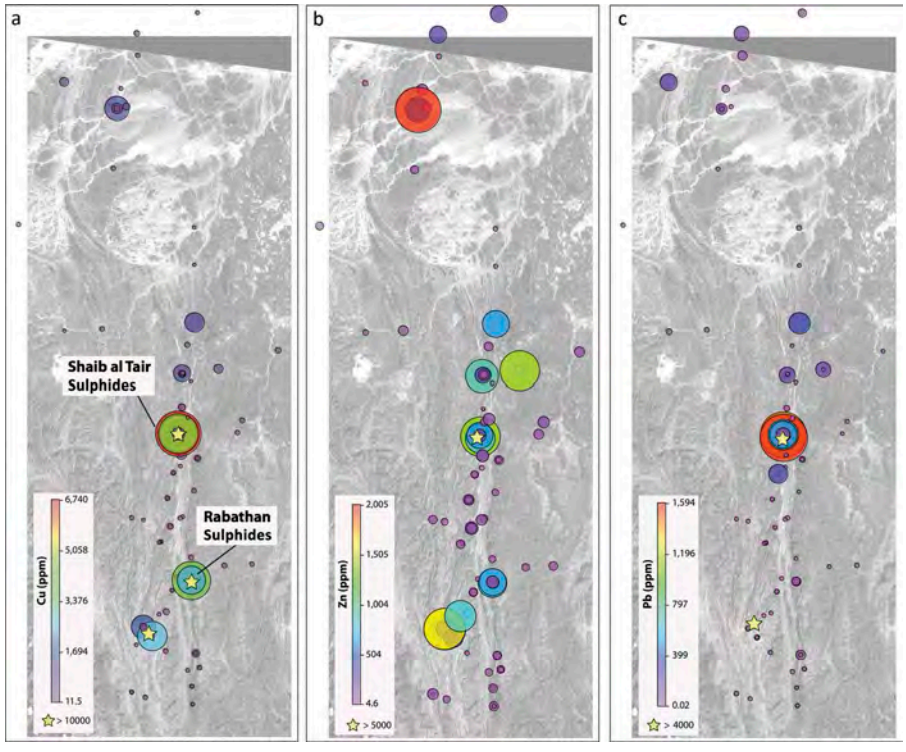

Figure 15. Proportional circle plots of selected elements overlying a Landsat 7 (Band 8) grey-scale image of the WBMD. (a) Cu; (b) Zn; and (c) Pb. Location of figure as in Figure 2.

REE profiles (in particular $[Gd/Yb]_{cn}$, and possibly Eu anomaly) and proximity to mineralization (Cu, Zn, and Pb shown in Figure 15).

The implications of the present research for mineral exploration are fourfold: (1) positive Eu anomalies in the massive sulphides reflect precipitation from high (>250° C) temperature hydrothermal fluid; spatial variations in the magnitude of the Eu anomaly could be used as a vector to mineralization at a regional scale (Genna *et al*. 2014a; Volesky *et al*. 2000; as also noted by Gale *et al*. 1997); (2) positive Eu anomalies in massive sulphides occur in samples with high Ba, Pb, and Zn contents; and (3) primary, concave-up REE patterns and positive Eu anomalies in massive sulphide are preserved through greenschist grade metamorphism and supergene weathering. Although Pérez-López *et al*. (2010) suggested that concave-up REE patterns in the Iberian Pyrite Belt are the result of preferential mobility of the middle REE during gossan formation, most WBMD altered felsic schists, cherts and some massive sulphides possess such concave-up REE patterns, suggesting that this is the result of hydrothermal alteration. Alternatively, it may be a primary lithological characteristic; however, the low pH values typical of gossanization (i.e. pH <3) are less likely to fractionate the MREE because of the predominance of REE-SO_4 complexes that show little variation in stability constant across the REE series (Leybourne *et al*. 2006), and we do not favour such an interpretation.

Conclusions

The geologic setting, host rock types and distributions together with their bulk geochemical compositions, together with characteristic metal enrichment suites (Cu, Pb, Zn, Ba), all indicate that the WBMD massive sulphides are VMS deposits that formed on or close to the seafloor in the Neoproterozoic. The volcanic rocks that host the SAT deposit are interpreted to have formed in an oceanic volcanic arc setting, and mineralization is comprised predominantly of Fe–Cu–Zn massive sulphides. Some samples of the hydrothermally altered schists in close proximity to both massive sulphide deposits (SAT and Rabathan) have positive Eu anomalies are enriched in Ba and Pb, and commonly display concave-up patterns on a chondrite-normalized REE plot, in contrast to the least altered host rock. The REE signatures of the massive sulphides, gossans, and least altered and altered host rocks provide information on the processes by which they formed. Furthermore, the REE, metal and other trace element data may have applications in exploration for volcanogenic massive sulphide deposits in the WBMD, other locations in Saudi Arabia, or other places where these types of deposits occur.

Acknowledgements

We thank Dr Mohammed A. Tawfiq, former President of the Saudi Geological Survey and the United States Geological Survey: Saudi Arabian Team (Jeff Doebrich, Ron Worl, and George Vranas) for their support and assistance during the fieldwork phase of this study and for providing personnel, equipment and vehicles necessary to complete the study. This work was supported by a National Aeronautics and Space Administration grant through JPL#961023/97001 to RJS. JMP thanks the Targeted Geoscience Initiative 4 Program of the Geological Survey of Canada (GSC); this is GSC contribution 20150441. Two anonymous journal reviewers are thanked for their careful reviews and constructive critiques that greatly improved the manuscript. We also thank editor Mohamed Abdelsalam for his editorial handling.

Disclosure statement

No potential conflict of interest was reported by the authors.

Funding

This work was supported by a National Aeronautics and Space Administration grant through JPL number 961023/97001 to RJS.

References

Abdelsalam, M.G., Liégeois, J.P., and Stern, R.J., 2002, The Saharan Metacraton: Journal of African Earth Sciences, v. 34, 3–4, p. 119–136. 10.1016/S0899-5362(02)00013-1

Abdelsalam, M.G., and Stern, R.J., 1996, Sutures and shear zones in the Arabian-Nubian shield: Journal of African Earth Sciences, v. 23, 3, p. 289–310. 10.1016/S0899-5362(97)00003-1

Agar, R.A., 1992, The tectono-metallogenic evolution of the arabian shield: Precambrian Research, v. 58, 1–4, p. 169–194. 10.1016/0301-9268(92)90118-8

Bamousa, A.O., 2013, Infracambrian superimposed tectonics in the Late Proterozoic units of Mount Ablah area, southern Asir Terrane, Arabian Shield, Saudi Arabia: Arabian Journal of Geosciences, v. 6, 6, p. 2035–2044. 10.1007/s12517-011-0490-5

Barrett, T.J., Jarvis, I., and Jarvis, K.E., 1990, Rare earth element geochemistry of massive sulfides-sulfates and gossans on the Southern Explorer Ridge: Geology, v. 18, p. 583–586. 10.1130/0091-7613(1990)018<0583:REEGOM>2.3.CO;2

Barrett, T.J., MacLean, W.H., Barrie, C.T., and Hannington, M.D., 1999, Volcanic sequences, lithogeochemistry, and hydrothermal alteration in some bimodal volcanic-associated massive sulfide systems: Reviews in Economic Geology, v. 8, p. 101–131

Barrett, T.J., MacLean, W.H., Cattalani, S., Hoy, L., and Riverin, G., 1991, Massive sulfide deposits of the Noranda area,

Quebec. III. The Ansil mine: Canadian Journal of Earth Science, v. 28, p. 1699–1730. 10.1139/e91-154

Barrie, C.T., Nielsen, F.W., and Aussant, C.H., 2007, The Bisha volcanic-associated massive sulfide deposit, western Nakfa Terrane, Eritrea: Economic Geology, v. 102, 4, p. 717–738. 10.2113/gsecongeo.102.4.717

Bau, M., Balan, S., Schmidt, K., and Koschinsky, A., 2010, Rare earth elements in mussel shells of the Mytilidae family as tracers for hidden and fossil high-temperature hydrothermal systems: Earth and Planetary Science Letters, v. 299, 3–4, p. 310–316. 10.1016/j.epsl.2010.09.011

Beaudoin, Y., and Scott, S.D., 2009, Pb in the PACMANUS seafloor hydrothermal system, eastern Manus Basin; numerical modeling of a magmatic versus leached origin: Economic Geology, v. 104, p. 749–758. 10.2113/gsecongeo.104.5.749

Beziat, P., and Donzeau, M., 1989, The Mamilah-Wadi Bidah mineral belt: geology and mineral exploration, Jeddah, Saudi Arabia, Directorate General of Mineral Resources, Ministry of Petroleum and Mineral Resources, p. 34.

Blain, C.F., 1977, Sulphide weathering and the evaluation of gossans in mineral exploration: Minerals, Science and Engineering, v. 9, 3, p. 119–150.

Boström, K., 1973, The origin and fate of ferromanganoan active ridge sediments: Stockholm Contributions in Geology, v. 27, p. 147–243

Boström, K., and Peterson, M.N.A., 1969, The origin of aluminum-poor ferromanganoan sediments in areas of high heat flow on the East Pacific Rise: Marine Geology, v. 7, p. 427–447. 10.1016/0025-3227(69)90016-4

Boyle, D.R., 1994, Oxidation of massive sulphide deposits in the Bathurst Mining Camp: natural analogues for acid drainage in temperate climates, *in* Alpers, C.N., and Blowes, D. W., eds., Environmental Geochemistry of Sulfide Oxidation: Washington, DC, American Chemical Society, p. 535–550.

Boyle, D.R., 1996, Supergene base metals and precious metals, *in* Eckstrand, O.R., Sinclair, W.D., and Thorpe, R.I., eds, Geology of Canadian Mineral Deposit Types: Ottawa, Ontario, Geological Survey of Canada, p. 92–108.

Boyle, D.R., 2003, Preglacial weathering of massive sulfide deposits in the Bathurst Mining Camp: Economic geology, geochemistry, and exploration applications, *in* Goodfellow, W.D., McCutcheon, S.R., and Peter, J.M., eds, Massive Sulphide Deposits of the Bathurst Mining Camp, New Brunswick, and Northern Maine, Littleton, CO, Society of Economic Geologists, Inc, p. 689–721.

Brophy, J.G., 2008, A study of rare earth element (REE)-SiO2 variations in felsic liquids generated by basalt fractionation and amphibolite melting: a potential test for discriminating between the two different processes: Contributions to Mineralogy and Petrology, v. 156, 3, p. 337–357. 10.1007/s00410-008-0289-x

Camp, V.E., 1984, Island arcs and their role in the evolution of the western Arabian Shield: Geological Society of America Bulletin, v. 95, 8, p. 913–921. 10.1130/0016-7606(1984)95<913:IAATRI>2.0.CO;2

Cortial, P., Lefevre, J.C., and Salih, H.M., 1985, Gold deposits related to the volcanosedimentary sequence of Ariab, Sudan, Prospecting in Areas of Desert Terrain, *in* Prospecting In Areas of Desert Terrain: Papers presented at the International Conference: London, Institution of Mining and Metallurgy, p. 155–159.

Cottard, F., Abdulhay, G.J., Artignan, D., Géïot, J.L., Roubichou, P., Trinquard, R., and Vadala, P., 1994, The Al Hajar gold deposit (Kingdom of Saudi Arabia): a newly discovered example of supergène enrichment from a massive sulfide deposit of late Proterozoic age: Chronique de la Recherche Miniere/Chronicle of Mineral Research and Exploration, v. 510, p. 13–24

Cottard, F., Braux, C., Cortial, P., Deschamps, Y., El Samani, Y., Hottin, A.-M., and Omar Younis, M., 1986, Polymetallic sulfide ore deposits and gold bearing mineralization in the Ariab District (Red Sea Hills, Sudan). History of the discovery, geology and main characteristics of the deposits: Chronique de la Recherche Miniere/Chronicle of Mineral Research and Exploration, v. 54, 483, p. 19–40.

Coumoul, A., Abdulhay, G., and Roubichou, P., 1989, Results of Gold Exploration in the Wadi Bidah District: Shaib at Tair Prospect, Directorate General of Mineral Resources, Ministry of Petroleum and Mineral Resources, Jeddah, Saudi Arabia, v. BRGM-OF-09-9, p. 59.

Craddock, P.R., and Bach, W., 2010, Insights to magmatic–hydrothermal processes in the Manus back-arc basin as recorded by anhydrite: Geochimica Et Cosmochimica Acta, v. 74, 19, p. 5514–5536. 10.1016/j.gca.2010.07.004

Craddock, P.R., Bach, W., Seewald, J.S., Rouxel, O.J., Reeves, E., and Tivey, M.K., 2010, Rare earth element abundances in hydrothermal fluids from the Manus Basin, Papua New Guinea: Indicators of sub-seafloor hydrothermal processes in back-arc basins: Geochimica Et Cosmochimica Acta, v. 74, 19, p. 5494–5513. 10.1016/j.gca.2010.07.003

Crerar, D.A., and Barnes, H.L., 1976, Ore solution chemistry V. Solubilities of chalcopyrite and chalcocite assemblages in hydrothermal solution at 200°C to 350°C: Economic Geology, v. 71, p. 772–794. 10.2113/gsecongeo.71.4.772

De Ronde, C.E.J., Massoth, G.J., Butterfield, D.A., Christenson, B. W., Ishibashi, J., Ditchburn, R.G., Hannington, M.D., Brathwaite, R.L., Lupton, J.E., Kamenetsky, V.S., Graham, I. J., Zellmer, G.F., Dziak, R.P., Embley, R.W., Dekov, V.M., Munnik, F., Lahr, J., Evans, L.J., and Takai, K., 2011, Submarine hydrothermal activity and gold-rich mineralization at Brothers Volcano: Kermadec arc, New Zealand, Mineralium Deposita, v. 46, p. 541–584. 10.1007/s00126-011-0345-8

Derry, L.A., and Jacobsen, S.B., 1990, The chemical evolution of Precambrian seawater: evidence from REE's in banded iron formations: Geochimica Et Cosmochimica Acta, v. 54, p. 2965–2977. 10.1016/0016-7037(90)90114-Z

Doebrich, J.L., Al-Jehani, A.M., Siddiqui, A.A., Hayes, T.S., Wooden, J.L., and Johnson, P.R., 2007, Geology and metallogeny of the Ar Rayn terrane, eastern Arabian shield: Evolution of a Neoproterozoic continental-margin arc during assembly of Gondwana within the East African orogen: Precambrian Research, v. 158, 1–2, p. 17–50. 10.1016/j.precamres.2007.04.003

Earhart, R.L., and Mawad, M.M., 1970, Geology and Mineral Evaluation of the Wadi Bidah District, Southern Hijaz Quadrangle, Kingdom of Saudi Arabia, Directorate General of Mineral Resources, Ministry of Petroleum and Mineral Resources, Jeddah, Saudi Arabia., v. USGS-OF-(IR)SA119.

Fleck, R.J., and Hadley, D.G., 1982, Ages and strontium initial ratios of plutonic rocks in a transect of the Arabian Shield: p. 43. U.S. Geological Survey Open File Report USGS-OF-03-38.

Fritz, H., Abdelsalam, M., Ali, K.A., Bingen, B., Collins, A.S., Fowler, A.R., Ghebreab, W., Hauzenberger, C.A., Johnson, P.R., Kusky, T.M., Macey, P., Muhongo, S., Stern, R.J., and Viola, G., 2013, Orogen styles in the East African Orogen: A review of the Neoproterozoic to Cambrian tectonic evolution: Journal of African Earth Sciences, v. 86, p. 65–106. 10.1016/j.jafrearsci.2013.06.004

Gale, A., Dalton, C.A., Langmuir, C.H., Su, Y., and Schilling, J.G., 2013, The mean composition of ocean ridge basalts: Geochemistry, Geophysics, Geosystems, v. 14, 3, p. 489–518. 10.1029/2012GC004334

Gale, G.H., Fedikow, M.A.F., and Dabek, L.B., 1997, The application of rare earth element analyses in the exploration for volcanogenic massive sulfide type deposits: Exploration and Mining Geology, v. 6, 3, p. 233–252.

Galley, A., Hannington, M., and Jonasson, I., 2007, Volcanogenic massive sulfide deposits, *in* Goodfellow, W. D., ed., Mineral Resources of Canada: A Synthesis of Major Deposit-types, District Metallogeny, the Evolution of Geological Provinces, and Exploration Methods: St. John's, Geological Association of Canada, Mineral Deposits Division, Special Publication No. 5, p. 141–161.

Galley, A.G., Watkinson, D.H., Jonasson, I.R., and Riverin, G., 1995, The subsea-floor formation of volcanic-hosted massive sulfide; evidence from the Ansil Deposit: Rouyn-Noranda, Canada, Economic Geology, v. 90, 7, p. 2006–2017. 10.2113/gsecongeo.90.7.2006

Gemmell, J.B., Sharpe, R., Jonasson, I.R., and Herzig, P.M., 2004, Sulfur isotope evidence for magmatic contributions to submarine and subaerial gold mineralization: Conical Seamount and the Ladolam Gold Deposit: Papua New Guinea, Economic Geology, v. 99, 8, p. 1711–1725. 10.2113/gsecongeo.99.8.1711

Genna, D., Gaboury, D., and Roy, G., 2014a, Evolution of a volcanogenic hydrothermal system recorded by the behavior of LREE and Eu: Case study of the Key Tuffite at Bracemac–McLeod deposits Matagami, Canada, : Ore Geology Reviews, v. 63, p. 160–177. 10.1016/j.oregeorev.2014.04.019

Genna, D., Gaboury, D., and Roy, G., 2014b, The Key Tuffite, Matagami Camp, Abitibi Greenstone Belt, Canada: petrogenesis and implications for VMS formation and exploration: Mineralium Deposita, v. 49, 4, p. 489–512. 10.1007/s00126-013-0499-7

Gibson, H.L., Watkinson, D.H., and Comba, C.D.A., 1983, Silicification: hydrothermal alteration in an Archean geothermal system within the Amulet rhyolite formation: Noranda, Quebec, Economic Geology, v. 78, 5, p. 954–971. 10.2113/gsecongeo.78.5.954

Gieré, R., 1993, Transport and deposition of REE in H2S-rich fluids: evidence from accessory mineral assemblages: Chemical Geology, v. 110, 1–3, p. 251–268. 10.1016/0009-2541(93)90257-J

Goodfellow, W.D., McCutcheon, S.R., and Peter, J.M., 2003, Massive Sulphide Deposits of the Bathurst Mining Camp, New Brunswick, and Northern Maine: Society of Economic Geologists, p. 925.

Graf, J.L., Jr., 1977, Rare earth elements as hydrothermal tracers during the formation of massive sulfide deposits in volcanic rocks: Economic Geology, v. 72, p. 527–548. 10.2113/gsecongeo.72.4.527

Greenwood, W.R., Anderson, R.E., Fleck, R.J., and Roberts, R. J., 1980, Precambrian geologic history and plate tectonic evolution of the Arabian Shield: Jeddah, Saudi Arabian Directorate General of Mineral Resources Bulletin 24, p. 35.

Greenwood, W.R., Hadley, D.G., Anderson, R.E., Fleck, R.J., and Schmidt, D.L., 1976, Late Proterozoic Cratonization in Southwestern Saudi Arabia: Philosophical Transactions of the Royal Society of London, v. A280, p. 517–520. 10.1098/rsta.1976.0010

Haas, J.R., Shock, E.L., and Sassani, D.C., 1995, Rare earth elements in hydrothermal systems: Estimates of standard partial molal thermodynamic properties of aqueous complexes of the rare earth elements at high pressures and temperatures: Geochimica Et Cosmochimica Acta, v. 59, p. 4329–4350. 10.1016/0016-7037(95)00314-P

Hamimi, Z., El-Sawy, E.-S.K., El-Fakharani, A., Matsah, M., Shujoon, A., and El-Shafei, M.K., 2014, Neoproterozoic structural evolution of the NE-trending Ad-Damm Shear Zone, Arabian Shield, Saudi Arabia: Journal of African Earth Sciences, v. 99, p. 51–63. 10.1016/j.jafrearsci.2013.09.010

Hannington, M.D., De Ronde, C.E.J., and Petersen, S., 2005, Sea-floor tectonics and submarine hydrothermal systems, *in* Hedenquist, J.W., et al., eds., Economic Geology One Hundredth Anniversary Volume, Littleton, Colorado, Society of Economic Geologists, Inc, p. 111–141.

Hanson, G.N., 1980, Rare earth elements in petrogenetic studies of igneous systems: Earth and Planeary Science Letters, v. 8, p. 371–406. 10.1146/annurev.ea.08.050180.002103

Hargrove, U.S., Stern, R.J., Kimura, J.I., Manton, W.I., and Johnson, P.R., 2006, How juvenile is the Arabian-Nubian Shield? Evidence from Nd isotopes and pre-Neoproterozoic inherited zircon in the Bi'r Umq suture zone: Saudi Arabia, Earth and Planetary Science Letters, v. 252, 3–4, p. 308–326. 10.1016/j.epsl.2006.10.002

Hodder, A.P.W., 1994, Rare earth mobility in young arc-type volcanic rocks from northern New Zealand; A comment to a paper by E. Kuschel and I.E.M. Smith: Geochimica Et Cosmochimica Acta, v. 58, p. 1389–1391. 10.1016/0016-7037(94)90393-X

Jackaman, B., 1972, Genetic and environmental factors controlling the formation of massive sulfide deposits of Wadi Bidah and Wadi Wassat, Saudi Arabia, Jeddah, Saudi Arabia, Directorate General of Mineral Resources, Ministry of Petroleum and Mineral Resources.

Johnson, P.R., 1999, Proterozoic geology of western Saudi Arabia, West Central Sheet: Jeddah, Saudi Arabian Deputy Ministry for Mineral Reources Open-file Report USGS-OF-99-2, 96 p.

Kato, Y., Yamaguchi, K.E., and Ohmoto, H., 2006, Rare earth elements in Precambrian banded iron formations: Secular changes of Ce and Eu anomalies and evolution of atmospheric oxygen: Geological Society of America Memoirs, v. 198, p. 269–289

Kerrich, R., and Wyman, D.A., 1996, The trace element systematics of igneous rocks in mineral exploration: an overview, *in* Wyman, D.A., ed., Trace Element Geochemistry of Volcanic Rocks: Applications for Massive Sulfide Exploration: St. John's, Geological Association of Canada, p. 1–50.

Kiilsgaard, T.H., Greenwood, W.R., Puffet, W.P., Naqvi, M.I., Roberts, R.J., Worl, R.G., Merghelani, H., Flanigan, V.J., and

Gazzaz, A.R., 1978, Mineral exploration in the Wadi Bidah District, 1972-1976, Kingdom of Saudi Arabia, Open-File Report. - ed.

Klinkhammer, G.P., Elderfield, H., Edmond, J.M., and Mitra, A., 1994, Geochemical implications of rare earth element patterns in hydrothermal fluids from mid-ocean ridges: Geochimica Et Cosmochimica Acta, v. 58, p. 5105–5113. 10.1016/0016-7037(94)90297-6

Koch-Mathian, J.Y., Tayeb, S., and Siddiqui, A.A., 1994, Results of copper-gold exploration in the Rabathan prospect (Wadi Bidah Belt), Technical Report BRGM-TR- 14-2 Ministry of Petroleum and Mineral Resources, Directorate General of Mineral Resources, Jiddah, Kingdom of Saudi Arabia.

Kuschel, E., and Smith, I.E.M., 1992, Rare earth mobility in young arc-type volcanic rocks from northern New Zealand: Geochimica Et Cosmochimica Acta, v. 56, 11, p. 3951–3955. 10.1016/0016-7037(92)90008-7

Large, R.R., Gemmell, J.B., Paulick, H., and Huston, D.L., 2001a, The alteration box plot: a simple approach to understanding the relationship between alteration mineralogy and lithogeochemistry associated with volcanic-hosted massive sulfide deposits: Economic Geology, v. 96, p. 957–971

Large, R.R., McPhie, J., Gemmell, J.B., Herrmann, W., and Davidson, G.J., 2001b, The spectrum of ore deposit types, volcanic environments, alteration halos, and related exploration vectors in submarine volcanic successions: Some examples from Australia: Economic Geology, v. 96, 5, p. 913–938.

Lemiere, B., 1989, Geochemistry of Volcanic Rocks of the Mamilah-Wadi Bidah Mineral Belt: Jeddah, BRGM-OF-09-5 App. A. Directorate General of Mineral Resources, Ministry of Petroluem and Mineral Resources, p. 12.

Lentz, D.R., 1996, Trace element systematics of felsic volcanic rocks associated with massive sulfide deposits in the Bathurst Mining Camp: petrogenetic, tectonic, and chemostratigraphic implications for VMS exploration, *in* Wyman, D. A., ed., Trace Element Geochemistry of Volcanic Rocks: Applications for Massive Sulfide Exploration: St. John's, Geological Association of Canada, p. 359–402.

Leybourne, M.I., Peter, J.M., Layton-Matthews, D., Volesky, J., and Boyle, D.R., 2006, Mobility and fractionation of rare earth elements during supergene weathering and gossan formation and chemical modification of massive sulfide gossan: Geochimica Et Cosmochimica Acta, v. 70, p. 1097–1112. 10.1016/j.gca.2005.11.003

Lydon, J.W., 2007, An overview of the economic and geological contexts of Canada's major mineral deposit types, *in* Goodfellow, W.D., ed., Mineral Resources of Canada: A Synthesis of Major Deposit-types, District Metallogeny, the Evolution of Geological Provinces, and Exploration Methods: St. John's, Geological Association of Canada, Mineral Deposits Division, Special Publication No. 5, p. 3–48.

Marcoux, E., Cottard, F., Recoche, G., El Samani, Y., Calvez, J.Y., and Deschamps, Y., 1989, Lead isotopic signatures of the polymetallic mineralization in the Ariab district, Red Sea Hills, northeastern Sudan: Journal of Geochemical Exploration, v. 32, 1–3, p. 315–317. 10.1016/0375-6742(89)90070-8

McDonough, W.F., and Sun, S.S., 1995, The composition of the Earth, *in* McDonough, W.F., Arndt, N.T., and Shirey, S., eds., Chemical evolution of the mantle, Amsterdam, Netherlands, Elsevier, p. 223–253.

McLennan, S.M., 1989, Rare earth elements in sedimentary rocks: influence of provenance and sedimentary processes: Reviews in Mineralogy and Geochemistry, v. 21, p. 169–200

Meschede, M., 1986, A method of discriminating between different types of mid-ocean ridge basalts and continental tholeiites with the Nb-Zr-Y diagram: Chemical Geology, v. 56, p. 207–218. 10.1016/0009-2541(86)90004-5

Michard, A., 1989, Rare earth element systematics in hydrothermal fluids: Geochimica Et Cosmochimica Acta, v. 53, p. 745–750. 10.1016/0016-7037(89)90017-3

Morgan, J.W., and Wandless, G.A., 1980, Rare earth element distribution in some hydrothermal minerals: evidence for crystallographic control: Geochimica Et Cosmochimica Acta, v. 44, 7, p. 973–980. 10.1016/0016-7037(80)90286-0

Nesbitt, H.W., and Young, G.M., 1982, Early proterozoic climates and plate motions inferred from major element chemistry of lutites: Nature, v. 299, 5885, p. 715–717. 10.1038/299715a0

Pan, Y.M., Fleet, M.E., and Barnett, R.L., 1994, Rare-Earth Mineralogy and Geochemistry of the Mattagami Lake Volcanogenic Massive Sulfide Deposit: Quebec, Canadian Mineralogist, v. 32, p. 133–147

Pérez-López, R., Delgado, J., Nieto, J.M., and Márquez-García, B., 2010, Rare earth element geochemistry of sulphide weathering in the São Domingos mine area (Iberian Pyrite Belt): A proxy for fluid–rock interaction and ancient mining pollution: Chemical Geology, v. 276, 1–2, p. 29–40. 10.1016/j.chemgeo.2010.05.018

Peter, J.M., and Goodfellow, W.D., 1996, Mineralogy, bulk and rare earth element geochemistry of massive sulphide-associated hydrothermal sediments of the Brunswick Horizon, Bathurst Mining Camp, New Brunswick: Canadian Journal of Earth Sciences, v. 33, p. 252–283. 10.1139/e96-021

Peter, J.M., Goodfellow, W.D., and Doherty, W., 2003, Hydrothermal sedimentary rocks of the Heath Steele Belt, Bathurst Mining Camp, New Brunswick: Part 2. Bulk and rare earth element geochemistry and implications for origin, *in* Goodfellow, W.D., McCutcheon, S.R., and Peter, J.M., eds., Massive Sulphide Deposits of the Bathurst Mining Camp, New Brunswick, and Northern Maine, Littleton, CO, Society of Economic Geologists, Inc., p. 391–415.

Peter, J.M., Leybourne, M.I., Scott, S.D., and Gorton, M.P., 2014, Geochemical constraints on the tectonic setting of basaltic host rocks to the Windy Craggy Cu-Co-Au massive sulphide deposit, northwestern British Columbia: International Geology Review, v. 56, 12, p. 1484–1503. 10.1080/00206814.2014.947335

Piercey, S.J., 2007, An overview of the use of petrochemistry in regional exploration for volcanogenic massive sulfide (VMS) deposits, Exploration 07; Exploration in the new millennium; conference program; Fifth Decennial International Conference on Mineral Exploration, p. 30.

Piercey, S.J., 2011, The setting, style, and role of magmatism in the formation of volcanogenic massive sulfide deposits: Mineralium Deposita, v. 46, 5–6, p. 449–471. 10.1007/s00126-011-0341-z

Piercey, S.J., 2015, A Semipermeable Interface Model for the Genesis of Subseafloor Replacement-Type. Volcanogenic Massive Sulfide (Vms) Deposits: Economic Geology, v. 110, 7, p. 1655–1660. 10.2113/econgeo.110.7.1655

Radain, A.A., Ali, S., Nasseef, A.O., and Abdel-Monem, A.A., 1987, Rb-Sr geochronology and geochemistry of plutonic

rocks from the Wadi Shuqub quadrangle, west-central Arabian Shield: Journal of African Earth Sciences, v. 6, 4, p. 553–568. 10.1016/0899-5362(87)90095-9

Ramsay, C.R., Basahel, A.N., and Jackson, N.J., 1981, Petrography, Ggeochemistry, and origin of the volcanose-dimentary succession between Jabal Ibrahim and Al-Aqiq, Saudi Arabia, Volume Vol. 4: Jeddah, Faculty of Earth Sciences Bulletin, King Abdulaziz University, p. 1–24.

Reeves, E.P., Seewald, J.S., Saccocia, P., Bach, W., Craddock, P. R., Shanks, W.C., Sylva, S.P., Walsh, E., Pichler, T., and Rosner, M., 2011, Geochemistry of hydrothermal fluids from the PACMANUS, Northeast Pual and Vienna Woods hydrother-mal fields, Manus Basin, Papua New Guinea: Geochimica Et Cosmochimica Acta, v. 75, 4, p. 1088–1123. 10.1016/j.gca.2010.11.008

Riofinex, 1979, An Assessment of the Mineral Potential of Part of the Wadi Bidah District.

Ryall, W.R., and Taylor, G.F., 1981, Gossan Evaluation Manual: Jeddah, RF-TR-01-3. Directorate General of Mineral Resources, Ministry of Petroluem and Mineral Resources, p. 176.

Sangster, D.F., and Abdulhay, G.J.S., 2005, Base metal (Cu-Pb-Zn) mineralization in the Kingdom of Saudi Arabia: Jeddah, Kingdom of Saudi Arabia, p. 128.

Sharpe, R., and Gemmell, J.B., 2001, Alteration Characteristics of the Archean Golden Grove Formation at the Gossan Hill Deposit: Economic Geology, v. 96, 5, p. 1239–1262. 10.2113/gsecongeo.96.5.1239

Solomon, M., and Walshe, J.L., 1979, The formation of massive sulfide deposits on the seafloor: Economic Geology, v. 74, p. 797–813. 10.2113/gsecongeo.74.4.797

Stern, R.J., and Bloomer, S.H., 1992, Subduction zone infancy: examples from the Eocene Izu-Bonin-Mariana and Jurassic California arcs: Geological Society of America Bulletin, v. 104, 12, p. 1621–1636. 10.1130/0016-7606(1992)104<1621:SZIEFT>2.3.CO;2

Stern, R.J., Mukherjee, S.K., Miller, N.R., Ali, K., and Johnson, P.R., 2013, ~750Ma banded iron formation from the Arabian-Nubian Shield-Implications for understanding Neoproterozoic tectonics, volcanism, and climate change: Precambrian Research, v. 239, p. 79–94. 10.1016/j.precamres.2013.07.015

Stoeser, D.B., and Camp, V.E., 1985, Pan-African microplate accretion of the Arabian shield: Geological Society of America Bulletin, v. 96, p. 817–826. 10.1130/0016-7606(1985)96<817:PMAOTA>2.0.CO;2

Stoeser, D.B., and Frost, C.D., 2006, Nd, Pb, Sr, and O isotopic characterization of Saudi Arabian Shield terranes: Chemical Geology, v. 226, 3–4, p. 163–188. 10.1016/j.chemgeo.2005.09.019

Sugahara, H., Sugitani, K., Mimura, K., Yamashita, F., and Yamamoto, K., 2010, A systematic rare-earth elements and yttrium study of Archean cherts at the Mount Goldsworthy greenstone belt in the Pilbara Craton: Implications for the origin of microfossil-bearing black cherts: Precambrian Research, v. 177, 1–2, p. 73–87. 10.1016/j.precamres.2009.10.005

Sverjensky, D.A., 1984, Europium redox equilibria in aqueous solution: Earth and Planetary Science Letters, v. 67, p. 70–78. 10.1016/0012-821X(84)90039-6

Syme, E.C., Bailes, A.H., Stern, R.A., Lucas, S.B., and Wyman, D. A., 1996, Geochemical characteristics of 1.9 Ga tectonostra-tigraphic assemblages and tectonic setting of massive sul-fide deposits in the Paleoproterozoic Flin Flon Belt, Canada, *in*, Wyman, D.A., ed., Trace Element Geochemistry of Volcanic Rocks: Applications for Massive Sulfide Exploration, Geological Association of Canada, p. 279–327.

Szymanski, R., 2012, Thermal Record of Tectonism in the Southwestern Arabian Plate with Special Focus on Red Sea Rift Development: Lawrence, KS, University of Kansas.

Taylor, G.F., 1987, Gossan and Ironstone Evaluation in Mineral Exploration: Rio de Janeiro, Brazilian Geochemistry Society, p. 78.

Thornber, M.R., and Taylor, G.F., 1992, The mechanisms of sulphide oxidation and gossan formation, *in* Butt, C.R.M., and Zeegers, H., eds., Handbook of Exploration Geochemistry: Elsevier Science B.V., p. 119–138.

Tornos, F., Peter, J.M., Allen, R., and Conde, C., 2015, Controls on the siting and style of volcanogenic massive sulphide deposits: Ore Geology Reviews, v. 68, p. 142–163. 10.1016/j.oregeorev.2015.01.003

Velasco, F., Herrero, J.M., Suárez, S., Yusta, I., Alvaro, A., and Tornos, F., 2013, Supergene features and evolution of gos-sans capping massive sulphide deposits in the Iberian Pyrite Belt: Ore Geology Reviews, v. 53, p. 181–203. 10.1016/j.oregeorev.2013.01.008

Volesky, J.C., Leybourne, M.I., and Boyle, D.R., 2000, Mobility of rare earth elements during weathering of massive sulfide deposits, Bathurst Mining Camp, New Brunswick, Canada, Reno, Nevada, Geological Society of America Annual Meeting.

Volesky, J.C., Stern, R.J., and Johnson, P.R., 2003, Geological control of massive sulfide mineralization in the Neoproterozoic Wadi Bidah shear zone, southwestern Saudi Arabia, inferences from orbital remote sensing and field studies: Precambrian Research, v. 123, 2–4, p. 235–247. 10.1016/S0301-9268(03)00070-6

Volesky, J.C., 2002, Massive sulfide deposits of the Wadi Bidah mineral district, Saudi Arabia; geologic control of mineralization, remote sensing and mineral exploration, geochemical exploration and petrogenesis. [Ph.D. thesis]: Texas, University of Texas at Dallas. 129 p.

Winchester, J.A., and Floyd, P.A., 1977, Geochemical discrimination of different magma series and their differentiation products using immobile elements: Chemical Geology, v. 20, p. 325–343. 10.1016/0009-2541(77)90057-2

Wood, D.A., 1980, The application of a Th-Hf-Ta diagram to problems of tectonomagmatic classification and to establishing the nature of crustal contamination of basaltic lavas of the British Tertiary volcanic province: Earth and Planetary Science Letters, v. 50, p. 11–30. 10.1016/0012-821X(80)90116-8

Ziab, A.M., and Ramsay, C.R., 1986, Geologic map of the Turabah Quadrangle, Sheet 21E.